Author Manuscript

Author Manuscript

Author Manuscript

Author Manuscript

HHS Public Access

Author manuscript

Cell Rep. Author manuscript; available in PMC 2023 December 20.

Published in final edited form as:

Cell Rep. 2023 November 28; 42(11): 113394. doi:10.1016/j.celrep.2023.113394.

Staphylococcus aureus α-toxin impairs early neutrophil localization via electrogenic disruption of store-operated calcium entry

Fan Yang[1], **Mingyi Suo**[1], **Homayemem Weli**[1,2], **Mason Wong**[1], **Alex Junidi**[2], **Celeste Cummings**[1], **Ryan Johnson**[1], **Kiara Mallory**[1], **Annie Y. Liu**[3], **Zev J. Greenberg**[1], **Laura G. Schuettpelz**[1], **Mark J. Miller**[3], **Cliff J. Luke**[1], **Gwendalyn J. Randolph**[2], **Bernd H. Zinselmeyer**[2], **Juliane Bubeck Wardenburg**[1], **Regina A. Clemens**[1,4,*]

[1]Department of Pediatrics, Washington University School of Medicine, St. Louis, MO 63110, USA

[2]Department of Pathology and Immunology, Washington University School of Medicine, St. Louis, MO 63110, USA

[3]Department of Medicine, Washington University School of Medicine, St. Louis, MO 63110, USA

[4]Lead contact

SUMMARY

The pore-forming *S. aureus* α-toxin (Hla) contributes to virulence and disease pathogenesis. While high concentrations of toxin induce cell death, neutrophils exhibit relative resistance to lysis, suggesting that the action of Hla may not be solely conferred by lytic susceptibility. Using intravital microscopy, we observed that Hla disrupts neutrophil localization and clustering early in infection. Hla forms a narrow, ion-selective pore, suggesting that Hla may dysregulate calcium or other ions to impair neutrophil function. We found that sub-lytic Hla did not permit calcium influx but caused rapid membrane depolarization. Depolarization decreases the electrogenic driving force for calcium, and concordantly, Hla suppressed calcium signaling *in vitro* and *in vivo* and calcium-dependent leukotriene B4 (LTB4) production, a key mediator of neutrophil clustering. Thus, Hla disrupts the early patterning of the neutrophil response to infection, in part through direct impairment of neutrophil calcium signaling. This early mis-localization of neutrophils may contribute to establishment of infection.

In brief

This is an open access article under the CC BY-NC-ND license (http://creativecommons.org/licenses/by-nd-nd/4.0/).

*Correspondence: clemensra@wustl.edu.

AUTHOR CONTRIBUTIONS

F.Y., M.S., H.W., R.J., C.C., R.A.C., M.J.M., Z.J.G., and K.M. performed experiments. F.Y. and M.S. assisted with manuscript preparation. F.Y., A.J., and B.H.Z. performed *in vivo* calcium imaging. M.W., A.Y.L., and R.A.C. performed *in vivo* image analysis. C.J.L., J.B.W., M.J.M., G.J.R., and L.G.S. provided experimental reagents, equipment, and expertise. R.A.C. supervised the project design and experiments and wrote the manuscript.

DECLARATION OF INTERESTS

The authors declare no competing interests.

SUPPLEMENTAL INFORMATION

Supplemental information can be found online at https://doi.org/10.1016/j.celrep.2023.113394.

Author Manuscript Author Manuscript Author Manuscript Author Manuscript

Yang et al. find that the pore-forming *S. aureus* α-toxin (Hla) disrupts the neutrophil response to infection by impairing calcium signaling. Acting as an ion-selective channel, Hla permits sodium influx leading to membrane depolarization and decreased electrogenic driving force for calcium entry. Mis-localization of neutrophils correlates with impaired bacterial control.

Graphical Abstract

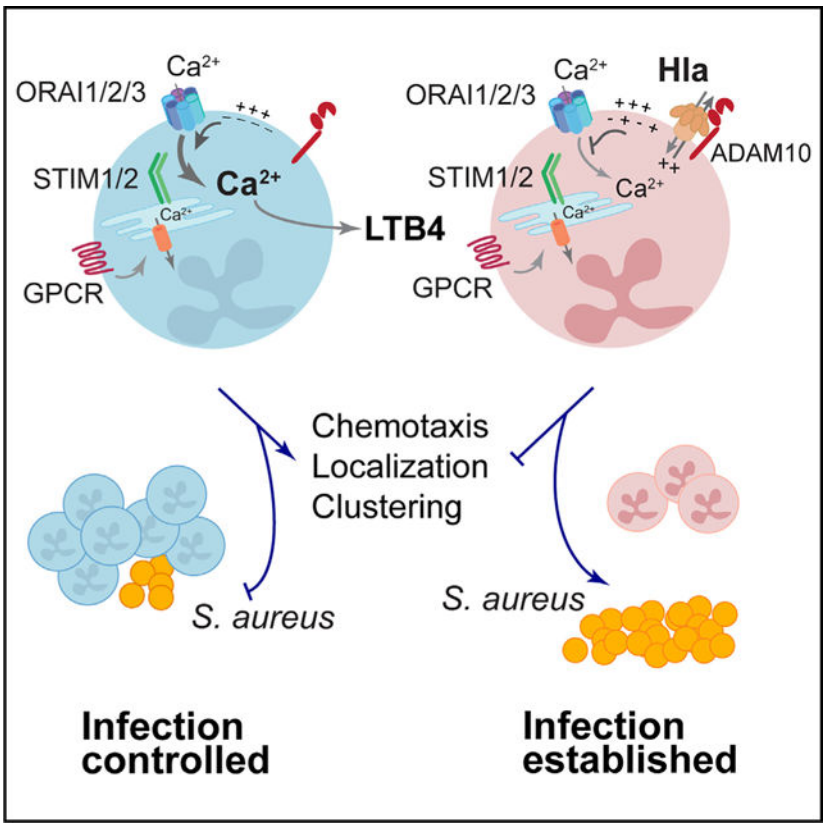

INTRODUCTION

Neutrophils are critical for host defense against *S. aureus*, evidenced by the severe infections occurring in patients with neutropenia or neutrophil dysfunction. These cells are first responders of the immune system and rapidly migrate to sites of infection, where they work to contain pathogens through production of bactericidal mediators. However, even in patients with intact immune systems, *S. aureus* is a highly pathogenic microorganism that is adept at subverting the immune response. The success of *S. aureus* in causing clinically significant disease is due in large part to virulence factors that impair host immune responses. Many of these virulence factors target neutrophil functions, including chemotactic G protein-coupled receptors (CHIPS, FLIPr, FLIPr-like, staphopain A); neutrophil-endothelial tethering via PSGL-1 (SEIX, SSL5); recognition by Toll-like receptor 2 (TLR2) (SSL3); opsonin-enhanced phagocytosis (protein A, SCIN); granule enzyme-mediated killing (serine protease inhibitors); and reactive oxygen species (ROS) production (superoxide dismutase).[1] The effort exerted by *S. aureus* to impair neutrophil

Author Manuscript Author Manuscript Author Manuscript Author Manuscript

function is further evidence of the importance of neutrophils in host defense against this pathogen.

S. aureus α-toxin (Hla) is a pore-forming toxin that is nearly ubiquitous in clinical isolates, and essential for pathogenesis in animal models of severe skin infection, pneumonia, sepsis, peritonitis, corneal infection, and central nervous system infection.[2] Hla is secreted by *S. aureus* as a water-soluble monomer, which binds to A disintegrin and metalloprotease 10 (ADAM10) to enable the assembly of the homo-heptameric toxin pore on the host cell surface.[3] Hla elicits cell-type-specific injury in a manner that reflects both the local concentration of Hla during infection and the level of ADAM10 expression on the host cell.[4] Epithelial and endothelial cells are highly sensitive to toxin-mediated lysis owing to higher ADAM10 expression. In contrast, neutrophils and other host immune cells exhibit a relative resistance to lysis, suggesting that the biologic action of Hla may not be solely conferred by lytic susceptibility.[5,6] The mechanisms by which sub-lytic concentrations of Hla alter target cell function are not well understood. In contrast to some other pore-forming toxins that form wide and permissive pores, the Hla pore is quite narrow. At ~1.2 nm, the Hla pore has features of an ion-selective channel, suggesting that sub-lytic levels of Hla could impact cell function via alteration of intracellular ion signaling.[7] The ion selectivity of this pore remains a matter of debate, however, particularly regarding calcium permeability. Several studies, including some in immune cells, have suggested that the Hla pore is permeable to calcium ions, whereas others suggest that calcium permeability may be dose dependent or indirectly triggered through activation of other receptors.[8] Changes in the cell membrane potential via movement of sodium or potassium ions could also indirectly impact the magnitude of calcium signals via alteration in the electrical driving force.

Calcium signaling is a central mediator of neutrophil function. Ligation of many neutrophil receptors, including tyrosine kinase-associated integrins, FcgR, or Dectin-1, and G proteincoupled receptors induces calcium influx and neutrophil activation.[9,10] Calcium entry into neutrophils occurs primarily by store-operated calcium entry (SOCE), whereby receptor activation initiates a signaling cascade culminating in activation of phospholipases that liberate diacylglycerol (DAG) and inositol triphosphate (IP_3) from membrane-bound phosphatidylinositol 4,5 bisphosphate (PIP_2)[11]. IP_3 binding to the endoplasmic reticulum (ER) IP_3 receptor releases “store” calcium from the ER, resulting in a transient increase in cytoplasmic calcium. Stromal interaction molecule (STIM) calcium sensors in the ER membrane undergo oligomerization and conformational change triggered by ER calcium depletion and gate calcium-release activated calcium (CRAC) channels, comprised of ORAI family members, in the plasma membrane to allow sustained calcium influx and activation of calcium-dependent cellular processes. SOCE is required for many neutrophil functional responses including phagocytosis, ROS production, degranulation, and production of cytokine and lipid inflammatory mediators.[11] Calcium flashes are also seen during chemotaxis, although the role of SOCE in neutrophil migration is not well established. We have previously demonstrated that mice lacking ORAI1/ORAI2 or STIM1 are susceptible to *S. aureus* skin infection and pneumonia,[12,13] supporting the notion that SOCE is important in the context of *S. aureus* infection. Given the central role of calcium signaling in neutrophil and immune cell function, this represents a possible target for pathogens to manipulate host defense.

Author Manuscript Author Manuscript Author Manuscript Author Manuscript

The effect of Hla on neutrophil function is not well understood, with few studies that directly examine the impact of Hla on neutrophil behavior. Some reports suggest that the toxin pore permits calcium entry and enhances neutrophil functions including phagocytosis and interleukin-1β (IL-1β) release,[6,14–16] while others report that the toxin may inhibit neutrophil function including migration.[17] *In vivo*, the impact of Hla on neutrophil behavior is similarly unclear, with one study reporting increased neutrophil infiltration during lung infection with an Hla-expressing strain, but another study showing that wild-type *S. aureus* skin infection produced decreased inflammatory mediators and neutrophil infiltration compared to infection with an Hla-strain.[18,19] The reason for heterogeneity in these findings is likely multifactorial. Neutrophils are highly sensitive cells, and it is possible that cell isolation techniques, experimental conditions, and/or purity of toxin contribute to varying results *in vitro*. Furthermore, *in vivo* studies are influenced by the model/tissue and time points examined. Regardless, additional investigation is required to better resolve how Hla impacts neutrophil function during infection.

We report here that pore formation with sub-lytic levels of Hla does not permit calcium influx but notably disrupts the neutrophil membrane potential. Depolarization potently inhibits SOCE and impairs early neutrophil migration, clustering, and localization to sites of *S. aureus* infection. These results identify a novel mechanism by which this toxin manipulates neutrophil function. This early mis-localization of neutrophils may allow for a critical period of unrestricted bacterial growth and contribute to establishment of infection.

RESULTS

Hla disrupts early neutrophil recruitment and clustering at an infected wound

Neutrophils are armed with an array of bactericidal mechanisms that are deployed to defend against invading microorganisms, including production of ROS and release of toxic granule enzymes. However, effective employment of these defenses requires the neutrophil to localize precisely to the site of infection. To test the impact of Hla on the spatial organization of the neutrophil response to infection, we created a wound model where a small superficial needle scratch is infected with wild-type (WT) or *Δhla S. aureus* on the pinnae of *Lyz2-EGFP* mice, which strongly express EGFP in neutrophils.[20] We then observed the pattern of the early neutrophil response (1.5–3 h post-infection [hpi]) by intravital 2-photon microscopy (2P-IVM) (Figures 1A and S1A). Neutrophils responded robustly to *Δhla S. aureus* infection, demonstrating directed migration toward the wound and forming dense and persistent clusters at the wound edge. In contrast, neutrophils responding to WT infection displayed meandering paths, with decreased speed, displacement, and track straightness compared to *Δhla* infection (Figures 1B–1F; Videos S1 and S2). Although clusters did form in WT infection, these clusters were generally smaller and were notably remote from the wound edge (Figures 1G–1I and S1B). Overall, neutrophil accumulation in the ~150 μm zone adjacent to the wound was impaired (Figures 1G–1I). Together, these observations suggest that Hla alters neutrophil migration and clustering early in *S. aureus* infection.

Author Manuscript Author Manuscript Author Manuscript Author Manuscript

Hla directly impairs neutrophil chemotaxis and clustering

In vivo, neutrophil behavior can be altered indirectly via effects on resident cells that produce cytokines or neutrophil chemoattractants or by direct effect on the neutrophil. To isolate the impact of Hla on the neutrophil, we utilized *in vitro* assays of neutrophil chemotaxis and clustering. Neutrophil chemotaxis toward the chemoattractant C5a was markedly impaired by sublytic doses of recombinant Hla, demonstrating decreased speed and directionality (Figures 2A–2G). To test the impact of Hla on neutrophil clustering, we embedded live WT or *Δhla S. aureus* in agarose and created bacterial agarose gel casts in chamber slides. Isolated mouse or human neutrophils were then added to the chamber slides and their behavior observed by video microscopy. Similar to 2P-IVM of the scratch wound, neutrophils exposed to *Δhla S. aureus* gels formed large clusters at the agarose edge within 30 min. Neutrophils incubated in wells with WT *S. aureus* formed fewer, smaller, and more transient clusters (Figures 2H–2L and S2A–S2D; Videos S3 and S4). The impact of Hla on human and mouse neutrophils was similar, suggesting that the toxin effect is conserved across species. To test whether differences in cell motility and clustering were due to cell death in WT infection, we added cell impermeant DAPI to the chambers in some experiments. The vast majority of neutrophils remained viable throughout this assay, and we observed no difference in the percentage of DAPI+ cells in WT and *Δhla* infection (Figures 2L, S2E, and S2F). These results suggest that Hla directly impacts neutrophil migration and clustering.

To further test whether the neutrophil clustering phenotype in vivo is due to a direct effect of the toxin on neutrophils, we turned to mice with deletion of *Adam10* driven by the MRP8-Cre, which is considered to drive neutrophil-specific deletion of genes. Interestingly, $Adam10^{Mrp8Cre}$ mice developed marked hair loss and skin inflammation starting at 6–7 weeks of age (Figures S3A and S3B). This inflammation was not driven by neutrophils or hematopoietic cells since creation of chimeras with $Adam10^{Mrp8Cre}$ bone marrow transferred into WT recipients did not result in inflammation (Figures S3C and S3D). MRP8 (S100A8) is highly expressed in neutrophils and drives more specific deletion in neutrophils compared to the myeloid LysM-Cre (*Lyz2Cre*).[21] Although it is not discussed extensively in the myeloid literature, there is well-documented expression of MRP8/S100a8 in mucosal and cutaneous epithelial cells, particularly in the setting of injury/inflammation.[22–24] Given the known role of ADAM10 in tissue and skin homeostasis,[25] we interpret these results as representing the effect of ADAM10 deletion in the skin. To circumvent this issue, we used 5- to 7-week-old $Adam10^{Mrp8Cre}$ mice for these experiments, prior to development of significant skin inflammation. Notably, $Adam10^{Mrp8Cre}$ x Lyz2-EGFP mice demonstrated robust cluster formation in WT *S. aureus* infection (Figures 2M–2P; Video S5), supporting the notion that Hla is directly impacting neutrophil behavior during infection. Plasmid complementation of Hla in the *Δhla S. aureus* (*Δhla/phla*) mutant recapitulated the *in vitro* and *in vivo* clustering phenotype elicited by *WT S. aureus*, confirming the specificity of *hla* deletion (Figures 2M–2P and S2G–S2J).

Hla disrupts neutrophil production of LTB4

Neutrophil clustering and swarming behavior are well-established phenomena where initial arrival of a few sentinel neutrophils at the site of sterile injury or infection is

Author Manuscript Author Manuscript Author Manuscript Author Manuscript

followed by rapid influx of additional neutrophils to the cluster. Neutrophil recruitment is amplified through autocrine and paracrine mechanisms of neutrophil crosstalk, and several chemoattractants and receptors involved in this process have been identified. The lipid mediator leukotriene B4 (LTB4) appears to play a central role in cluster formation.[26,27] LTB4 production can be initiated via several neutrophil receptors, where activation of calcium-dependent phospholipases liberates arachidonic acid from the membrane, which is then converted by the enzyme 5-lipoxygenase (5-LO) into downstream lipid mediators including LTB4. Signaling through the LTB4 receptor BLT1, a G protein-coupled receptor expressed on neutrophils, results in calcium influx, neutrophil migration, and also more LTB4 production, thus creating an LTB4- and calcium-dependent amplification loop. To test whether LTB4 was required for neutrophil clustering in response to *Δhla S. aureus*, we used the 5-LO inhibitor zileuton. In the presence of the inhibitor, *in vitro* neutrophil clustering was significantly decreased with *Δhla*, but not WT, *S. aureus* (Figures 3A–3E; Videos S3 and S6). Furthermore, neutrophil production of LTB4 was markedly suppressed by Hla (Figure 3F), suggesting that the toxin may inhibit neutrophil clustering via disrupting LTB4 production. Since calcium signaling is anticipated to participate in LTB4 production and also signaling through the LTB4 receptor, we next tested whether calcium influx was altered by Hla. Indeed, pre-incubation of neutrophils with Hla inhibited calcium influx triggered by both C5a and LTB4 (Figures 3G–3J), suggesting that Hla disrupts calcium-dependent LTB4 synthesis. We have previously demonstrated that neutrophil LTB4 release requires SOCE[13]; therefore we tested whether neutrophil chemotaxis and clustering require SOCE using neutrophils with deletion of STIM1 and STIM2, ER calcium sensors required for SOCE. Notably, STIM1/2-deficient neutrophils demonstrated impaired directionality during chemotaxis (Figures 3K–3N) and impaired cluster formation in the presence of Δhla, but not WT, *S. aureus* (Figures 3O–3S), supporting the notion that neutrophil chemotaxis and clustering during *S. aureus* infection require SOCE.

Hla inhibits neutrophil SOCE

We next turned to better understand the impact of Hla on neutrophil calcium levels, particularly in light of the conflicting reports regarding the permeability of the Hla pore to calcium.[8,15,28] We first examined whether the toxin pore permits calcium entry into neutrophils treated with sub-lytic concentrations of Hla. Application of Hla to neutrophils did not permit calcium influx (Figures 4A and 4B). Calcium entry via SOCE occurs in two phases: (1) receptor activation of a signaling cascade results in ER calcium release via IP3 receptors. (2) ER calcium depletion activates STIM calcium sensors, which gate plasma membrane CRAC channels to allow for entry of calcium from the extracellular space. To discern which step of calcium entry is affected by Hla, we stimulated neutrophils with ionomycin (ER calcium ionophore) first in calcium-free media to isolate ER calcium release, followed by addition of calcium to the media to examine calcium entry via plasma membrane channels. ER calcium release was unchanged by Hla, whereas plasma membrane calcium entry was significantly suppressed, suggesting that plasma membrane calcium flux, but not proximal ER calcium store release, is impacted by Hla (Figures 4C–4E). Suppression of calcium influx requires Hla pore formation and binding to its receptor ADAM10, as calcium entry in the presence of the Hla_{H35L} mutant, which does not form a functional pore, or in ADAM10-deficient neutrophils was unchanged compared with control (Figures 4F–4I).

Author Manuscript Author Manuscript Author Manuscript Author Manuscript

Ion flux through Hla pore depolarizes the neutrophil membrane potential

Calcium influx through CRAC channels is determined by three primary factors: (1) composition and permeability of the channels, (2) calcium chemical gradient (extracellular vs. intracellular calcium concentration), and (3) electrical driving force (i.e., membrane potential). Since the neutrophil channel expression and calcium gradient should be consistent in these experiments, we focused on the cell membrane potential. Immune cells utilize endogenous channels to modulate the cell membrane potential during cell stimulation. T cells express calcium- and voltage-gated potassium channels that, when open, permit potassium efflux, which hyperpolarizes the membrane potential and drives calcium influx.[29,30] We have also demonstrated that the membrane potential is an important regulator of neutrophil SOCE.[13] To determine how Hla impacts the neutrophil membrane potential, we utilized the membrane-potential-sensitive dye DiBAC4(3). Upon addition of sub-lytic doses of Hla, neutrophils rapidly depolarized (Figures 5A and 5B). Depolarization again required pore formation and Hla binding to ADAM10 (Figures 5C–5F). Based on a calibration of the DIBAC4(3) dye using the potassium ionophore valinomycin, we estimate that the observed ~3-fold change in fluorescence corresponds to a depolarization to −20 to 30 mV from a resting potential of ~−70 mV.[13] The major cellular ions that regulate the cell membrane potential are sodium, potassium, and chloride. Increased permeability of the cell membrane to any given ion tends to move the membrane potential toward the ion's equilibrium potential, where the electrical gradient and chemical gradient are balanced. For potassium and chloride, these are −105 and −65 mV, respectively; thus, the movement of these ions along their concentration gradient does not tend to drive depolarization. In contrast, the chemical and electrical gradients of sodium drive the positively charged ion into the cell, toward its equilibrium potential of +60 mV. To determine whether sodium influx contributes to Hla-mediated depolarization, we first tested the change in membrane potential in sodium-free media. Indeed, in the absence of sodium, there was significantly less depolarization with Hla (Figures 5G and 5H). Additionally, Hla application led to increased fluorescence of a sodium indicator, similar to the known sodium ionophore gramicidin (Figure 5I). Together, these results suggest that Hla-mediated neutrophil depolarization is driven at least in part by sodium influx.

Hla disrupts neutrophil calcium signaling in vivo

Since we observed that Hla disrupts migration and clustering of neutrophils both *in vivo* and *in vitro* and that the toxin also disrupts influx of calcium via SOCE and impairs calcium-dependent production of LTB4, we next asked whether calcium signaling is impaired by Hla *in vivo*. Salsa6f is a germline-encoded ratiometric calcium indicator where the calcium-sensitive GCaMP6f expression is linked to tdTomato via a V5 epitope tag and inserted into the *Gt(ROSA)26Sor* locus with a floxed STOP cassette to allow Cre-driven expression in target cells.[31] We crossed *Salsa6f*$^{flox/flox}$ to both Lyz2-Cre and MRP8-Cre mice to drive expression in neutrophils. Both Cre lines created adequate Salsa6f expression in neutrophils to visualize calcium flashes by 2P-IVM but also demonstrated expression in other cells. *Salsa6f*^{Lyz2Cre} mice exhibited additional expression in skin myeloid cells and structures that appear by morphology to be neurons. Neuronal activity of Lyz2-Cre has been previously reported.[32] Interestingly, *Salsa6f*^{Mrp8Cre} mice displayed strong Salsa6f expression in hair follicles, consistent with the hair/skin phenotype that we observed in *Adam10*^{MRP8Cre} mice.

Author Manuscript Author Manuscript Author Manuscript Author Manuscript

Neutrophils were easily identified in both mice given their distinctive cell morphology and motility. Adjacent to the *S. aureus* wound, neutrophil calcium spikes were visible in both WT and *Δhla S. aureus* infection; however, spike amplitude was significantly greater in neutrophils responding to *Δhla* infection (Figure 6; Videos S7, S8, S9, and S10). These findings support the notion that Hla impairs neutrophil migration and localization to the wound via disruption of neutrophil SOCE.

Disruption of early neutrophil localization in *S. aureus* infection is associated with impaired bacterial control

Given our observation that Hla disrupts neutrophil recruitment and localization to the wound in skin infection, we reasoned that this mechanism is likely important in any situation where anatomical constraints create an Hla concentration gradient emanating from the focus of infection. *S. aureus* pneumonia is a clinically important invasive infection that results in significant morbidity and mortality in humans. Initial infection is typically established in the alveolus, followed by bacterial invasion into the lung interstitium. Neutrophils are recruited into the alveoli in an attempt to contain the bacteria. We hypothesized that early in infection, bacterial production of Hla serves as a repellant for neutrophil migration into the alveolar space, safeguarding bacterial survival. To test this, we administered a lethal dose (2.4×10^8) of WT or *Δhla S. aureus* intranasally in WT mice and examined neutrophil numbers in the bronchoalveolar lavage (BAL). There were significantly more BAL neutrophils at 4 and 6 hpi in *Δhla* vs. WT infection (Figures 7A and 7B). Notably, decreased neutrophil accumulation in both WT *S. aureus* skin infection and pneumonia was correlated with increased *S. aureus* colony-forming unit (CFU) recovery early in infection (Figures 7C–7E), suggesting that neutrophil localization is functionally important for the outcome of infection. To determine whether this early neutrophil recruitment in *Δhla* infection was dependent on calcium signaling, we examined neutrophil migration and bacterial control in mice with impaired neutrophil SOCE (*Stim1/Stim2*^{Mrp8Cre} mice). Indeed, in response to *Δhla S. aureus*, neutrophil recruitment to the BAL and bacterial control were impaired in *Stim1/Stim2*^{Mrp8Cre} mice (Figures 7F–7H). Together, these results support the conclusion that Hla impairs early calcium-dependent neutrophil localization both to superficial skin infection and in lethal *S. aureus* pneumonia.

DISCUSSION

Despite a seemingly robust neutrophil response to infection, *S. aureus* is quite adept at establishing infection, leading to over 0.5 million hospitalizations per year.[33] Hla is known to be a key virulence factor that is conserved across multiple methicillin-sensitive and methicillin-resistant clinical isolates. It is clear that above a threshold concentration, Hla lytic function contributes to cell death, tissue injury, and disease pathogenesis; however, less is known about how sub-lytic concentrations of Hla impact cell function, particularly in immune cells that are relatively resistant to lysis, and how this contributes to disease. Our study provides fundamental new insight into how α-toxin disrupts early neutrophil migration and localization at the site of infection. Furthermore, we demonstrate a novel mechanism by which the ion-selective toxin pore disrupts the neutrophil membrane potential and impairs SOCE, thus impairing calcium-dependent neutrophil migration, clustering, and host defense.

Author Manuscript Author Manuscript Author Manuscript Author Manuscript

While other virulence factors have been visualized by intravital microscopy to alter neutrophil recruitment,[34,35] to our knowledge, a direct effect of Hla on neutrophil recruitment *in vivo* has not been reported. Several groups have observed that Δhla *S. aureus* or toxin neutralization enhances neutrophil accumulation in established skin infection (1 day post-infection [dpi]).[18,36] Furthermore, Abtin et al. demonstrated that Hlamediated lysis of perivascular macrophages decreases production of key chemokines and impairs neutrophil extravasation and recruitment to skin infection at 12 hpi.[37] However, how Hla impacts the early patterning of the neutrophil response to infection, and whether Hla has a direct effect on neutrophils *in vivo*, has not been defined. It is essential to note that *S. aureus* encodes multiple pore-forming cytotoxins (PFTs) classified as bicomponent leukocidins, including LukAB, LukED, LukSF-PV, HlgAB, and HlgCB. These toxins bear structural and functional similarity to Hla and elicit neutrophil injury via expression of well-characterized cell surface receptors.[38] Interestingly, many of these receptors are G protein-coupled receptors (GPCRs)/chemokine receptors, which are activated upon toxin binding. These toxins may also elicit a complex interplay of receptor activated calcium influx and pore-facilitated membrane potential alterations that modulate SOCE and neutrophil function at sub-cytolytic concentrations and synergize with Hla to impair neutrophil function. Given the receptor specificity of each of these PFTs, neutrophil susceptibility to the independent or combined action of these toxins *in vivo* is expected to exhibit not only species selectivity but may also reflect the tissue site of infection and the state of maturity or priming of the neutrophil. As such, what may appear to be redundancy of this family of PFTs may in fact confer exquisite biologic specificity that enables the success of *S. aureus* across distinct tissue microenvironments.

The ear wound model used in this study was developed with the goal of visualizing neutrophil recruitment to a defined area. This model resembles the clinically relevant scenario where bacteria contaminate a superficial wound and avoids injection of a bolus of bacteria that creates separation of tissue planes that may lead to dispersion of bacteria or change the diffusion of toxin.[34,35,39] The spatial resolution of this model enabled visualization of markedly altered neutrophil localization in early WT *S. aureus* infection. Although the absolute distance between the wound and the neutrophils in WT infection is relatively small (50–150 μm), from the perspective of the bacteria, this distance is vast. We observed very few neutrophils actually reaching the wound edge; thus, the opportunity for these cells to physically ingest and kill bacteria is limited. *S. aureus* has a rapid doubling time in rich media of 20 min. Although the growth rate is slower in other conditions, unimpeded bacterial replication for even a few hours has the potential to compound the challenge for host defense and allow for infection progression. Indeed, impaired early neutrophil localization to the scratch wound was associated with increased CFU recovery. Furthermore, neutrophil recruitment to the alveolus and bacterial control were also impaired in WT *S. aureus* lung infection, suggesting that this mechanism of Hla-mediated neutrophil impairment is relevant at any site of infection where anatomic constraints create an Hla gradient. It is important to note that several other groups have assessed CFU recovery in WT vs. *Δhla S. aureus* skin infection using the more common model of intradermal injection of bacteria, and to our knowledge, none have observed a difference in CFUs at 48 h or less.[4,18] We hypothesize that the large inoculum and volume used (30–50 μL) in these studies

Author Manuscript Author Manuscript Author Manuscript Author Manuscript

overload the early host response, thus masking any difference in early neutrophil-mediated bacterial killing. We propose that this time period of focus, 1.5–3 h after infection, is a critical period for paracrine amplification of neutrophil recruitment and patterning of the host response to infection. Additional studies are needed to investigate how the initial patterning of the neutrophil response evolves during the next phase of infection. Although during these first hours of infection, we observe minimal contact between neutrophils and the wound/bacteria in WT infection, presumably some neutrophils will gain access to the wound at later time points. Since calcium signaling is required for neutrophil bactericidal functions including phagocytosis, ROS production, and degranulation,[12,13,40] it will be necessary to determine whether Hla-mediated impairment of these responses compounds the effect of neutrophil mis-localization at later stages of infection.

Given the essential role of SOCE in immune cell function, this pathway poses an opportunity for pathogens to manipulate as a mechanism of immune evasion. For instance, helminths have been shown to secrete soluble ligands that inhibit macrophage SOCE and dampen the inflammatory response.[41] Epstein-Barr virus can enhance SOCE in B cells through upregulation of ORAI1, and enhanced calcium flux is suggested to play a role in the viral life cycle, as well as immortalization of the B cell.[42] Additionally, some viral and bacterial toxins are ion-permeable pores that can either induce or modulate SOCE.[28,43] We now show here that Hla targets neutrophil calcium signaling via modulation of the neutrophil membrane potential. To our knowledge, this is the first study to demonstrate this finding in immune cells. As such, this finding poses many additional questions, including whether this effect of the toxin is restricted to neutrophils or extends to other immune cells and whether this is a conserved mechanism utilized by other pore-forming toxins to manipulate neutrophil activity. Our findings also expand on previous studies to demonstrate that SOCE supports neutrophil clustering and directional migration. We have previously shown that ORAI1 and ORAI2 are important for LTB4 production, a key mediator of neutrophil clustering.[13] Furthermore, Khassen et al. recently demonstrated that neutrophil cluster formation is associated with calcium signals and that forced activation of SOCE utilizing and optogenically activatable STIM1 is able to induce spontaneous cluster formation.[44] We therefore extend these findings to establish a direct role for STIM1 and STIM2 in neutrophil clustering. Previous studies from our lab and others have generated mixed results on the importance of SOCE for neutrophil migration. I*n vivo*, at times points where inflammation/infection are well established, neutrophils lacking STIM1 or STIM1/STIM2 accumulate at the site of infection as well as WT neutrophils.[12,40] *Stim1/2*$^{-/-}$ neutrophils also migrated similarly to WT in a Transwell assay; however, the sensitivity of these *in vivo* and *in vitro* assays is limited. In contrast, Steinckwich et at. demonstrated that STIM1 is required for neutrophil recruitment to psoriasis lesions *in vivo*.[45] Here, we observe that SOCE mutants have impaired chemotaxis and clustering by video microscopy and impaired early neutrophil recruitment in lung infection, supporting a role for SOCE in neutrophil migration and localization at the site of infection. Also, coupled with our previous work demonstrating the susceptibility of ORAI1/ORAI2- and STIM1-deficient mice to skin and pulmonary infections, this study further demonstrates the importance of calcium signaling for the neutrophil response to *S. aureus*.[12,13]

Author Manuscript Author Manuscript Author Manuscript Author Manuscript

Limitations of the study

There are several important limitations to note for this study. First, we used distinct approaches to determine whether the phenotype that we observed *in vivo* results from a direct effect of the toxin on neutrophils or an indirect effect via toxin impact on another cell. Our results demonstrate that Hla certainly directly alters neutrophil function; however, *in vivo*, all resident and infiltrating cells are exposed to Hla, and it is possible that Hla also impacts the production of pathogen-associated molecular patterns (PAMPs) or chemokines that direct neutrophil migration. Identifying additional cell types that contribute to this phenotype will require observation of neutrophil behavior in mice with cell-type-specific disruption of Hla-ADAM10 interaction. Next, our study demonstrates that Hla impairs neutrophil SOCE and that the neutrophil behaviors that are altered in the presence of Hla are SOCE dependent. Thus, we propose that Hla disrupts neutrophil function primarily via altered calcium signaling. However, it is certainly possible that the toxin impacts neutrophil responses via additional mechanisms. Changes in the membrane potential or intracellular sodium may alter neutrophil function independent of calcium signaling. Also, we do not directly investigate the role of ADAM10 activation on neutrophil function, yet pore formation is known to trigger the rapid activation of ADAM10 enzymatic function and host tissue injury by ADAM10-mediated proteolysis.[5,46] Thus, ADAM10 activation may also contribute to the modulation of neutrophil behavior. This will require further study to dissect the relative contributions of the electrogenic effects of the toxin vs. ADAM10 activation. Finally, there are many important differences between human and mouse neutrophils, specifically as some *S. aureus* toxins, such as Panton-Valentine leukocidin (PVL), are not active on mouse neutrophils due to species-specific differences in the toxin receptors.[47–49] We demonstrate here that the inhibition of clustering by α-toxin-producing *S. aureus* is similar to mouse and human neutrophils, suggesting that the effect of Hla is preserved across species; however, attention to species differences is warranted in future studies.

Lastly, it is important to stress our finding that the MRP8-Cre drives deletion of ADAM10 in non-hematopoietic cells, leading to lethal skin inflammation. This is also visualized in the *Salsa6f*^{MRP8Cre} mice, where there is strong Cre-mediated expression of Salsa6f in hair follicles. To our knowledge, MRP8-Cre-driven deletion leading to a significant non-hematopoietic phenotype has not been widely described. These findings are incredibly important for consideration of results from past and future studies utilizing the MRP8-Cre for “neutrophilspecific” deletion of genes, particularly those genes like ADAM10 that have a broad expression and important function in many tissues. Cre-driven deletion is a useful tool for studying the contributions of a gene to the function of a specific cell types; however, these results reinforce the need for careful interpretation of such studies.

STAR★METHODS

RESOURCE AVAILABILITY

Lead contact—Further information and requests for resources and reagents should be directed to and will be fulfilled by the lead contact, Regina Clemens (clemensra@wustl.edu).

Author Manuscript Author Manuscript Author Manuscript Author Manuscript

Materials availability—Further information and requests for resources and reagents should be directed to and will be fulfilled by the lead contact, Regina Clemens (clemensra@wustl.edu).

Data and code availability—All data reported in this paper will be shared by the corresponding author upon request. This paper does not report original code. Any additional information required to reanalyze the data reported in this paper is available upon reasonable request from the corresponding author, Regina Clemens (clemensra@wustl.edu).

EXPERIMENTAL MODEL AND STUDY PARTICIPANT DETAILS

Mice—Mice (see Key resources table list) were maintained on the C57Bl/6J background and crossed as indicated. 8–12 weeks old male and female mice were used for experiments unless otherwise indicated. Controls were predominantly littermate (*flox/flox*) mice or age and sex matched C56Bl6/J. Mice were maintained in AAALAC accredited, specific pathogen-free barrier facilities at Washington University and used in accordance with approved IACUC protocols and the 8th edition Guide for the Care and Use of Lab Animals.

Experiments were conducted using neutrophils from 2 healthy adults between the ages of 30–50 years. One subject was male, one was female. All studies were approved by the Institutional Review Board at Washington University in St. Louis.

Bacterial strains and culture—Bacterial strains and sources are listed in Key resources table. We used the *S. aureus* USA300/LAC strain and two isogenic Hla deficient strains in these experiments: 1. Hla-deficient USA300/LAC strain containing a transposon insertion in the *hla* locus (*hla::erm*)[52] and 2. Hla-deficient USA300/LAC strain with a genetic deletion of the *hla* locus (*Δhla*) constructed using the pJB38 plasmid (see STAR Methods details below).[53] No significant phenotypic differences were observed between these mutants, both of which were confirmed to result from single gene deletion events via complementation. For complementation studies, mutant staphylococci were transformed with the pOS1 plasmid encoding *hla* (termed *phla*) then verified for restoration of Hla expression via protein expression and functional assessment of Hla-mediated lysis of rabbit red cells. *S. aureus* strains were cultured in tryptic soy broth (TSB), in the presence of erythromycin (100 μg/mL, *hla::erm*) or chloramphenicol (20 μg/mL, *hla::erm*/phla, *Δhla*/p*hla*, YFP-expressing strains) if indicated for selection.

METHOD DETAILS

Mouse neutrophil isolation—Bone marrow neutrophils were isolated from mice by using a single-step Percoll gradient.[13] Bone marrow cells were flushed using HBSS/20mM HEPES buffer from the femurs and tibias then subjected to a hypotonic lysis step with 0.2% sodium chloride for 30 s. Tonicity was restored with 1.6% sodium chloride and cells filtered through a 70μm cell strainer. Cells resuspended in HBSS/HEPES were gently layered over an equal volume of 62% Percoll and spun at room temperature (no brake, 1300g) for 30 min. The mononuclear layer was removed at the media/Percoll interface and neutrophils recovered from the loose cell pellet “swirl”.

Author Manuscript Author Manuscript Author Manuscript Author Manuscript

Human neutrophil isolation—Human neutrophils were isolated from blood collected in EDTA tubes using EasySep Direct Human Neutrophil Isolation Kit (StemCell) per the manufacturer's protocol. Neutrophil purity was >95% as determined by flow cytometry.

USA300/LAC hla knock-out strain construction—*Hla* flanking sequence PCR was performed using the primers listed below. The product of the PCR was cloned to a pJB38 vector at the EcoRI and KpnI restriction sites. Plasmids were generated in DH5α *Escherichia coli* and transferred to a restriction-deficient *Staphylococcus aureus* strain RN4220. Vectors were isolated from RN4220 and transformed into an electrocompetent *S. aureus* USA300/LAC strain. *Hla allelic* replacement was performed.[53] Recombination strains containing the mutagenesis plasmid were struck onto tryptic soy agar (TSA) supplemented with 10 μg/mL of chloramphenicol and incubated at 44°C overnight. Large colonies were plated onto TSA with chloramphenicol a second time and then incubated at 44°C overnight. These single recombinants were used to inoculate 3mL of tryptic soy broth (TSB) and incubated at 30°C without selection to promote a second round of recombination and plasmid loss. After several days of serial dilutions, cultures were plated on TSA with 100 ng/mL of anhydrotetracycline, and the resulting colonies were plated in replicate onto TSA alone, TSA with erythromycin, and TSA with chloramphenicol to identify cells that had undergone a second recombination event and lost the plasmid. Erythromycin-sensitive colonies were screened by PCR to confirm the absence of *hla* gene using Hla-S1 and Hla-S2 primers. The lack of Hla production was also confirmed by the absence of a hemolytic zone on blood agar. The list of primers used for Hla allelic replacement is included in the Key resources table section.

Chimera generation—Chimeric mice were generated by transplanting whole bone marrow cells from Adam10flox/flox x MRP8Cre *or* Adam10flox/+ x MRP8Cre (CD45.2) mice into WT (CD45.1) recipients. A total of 2×10^6 cells were injected retro–orbitally into lethally irradiated recipients (550cGy × 2, 4 h apart). Cells were allowed to engraft for 6 weeks prior to analysis for chimerism. Mice were followed for 16 weeks after transplantation for development of skin lesions.

Ear infection model—Following a 1:100 dilution of an overnight culture into fresh tryptic soy broth, WT or *Δhla S. aureus* were grown with shaking at 37°C to an optical density 1.4 at 600nm (2.5×10^9 CFU/mL, early stationary phase to optimize Hla production). 50mL culture aliquots were centrifuged and bacterial pellets were resuspended in 1mL of PBS. Mice were sedated using isoflurane controlled by an anesthetic machine (Midmark, Dayton, OH) and a metal clip was gently placed on the ear to stabilize the ear and provide a guide for a reproducible needle scratch. A 5μL droplet of concentrated bacterial suspension (~1.5×10^9 CFU) was added onto the ear surface and a ~2–3mm wound was induced manually using a 27G x ½" needle to scratch through the bacterial suspension. The residual bacterial droplet was then blotted off using a Kimwipe and the site examined for minor bleeding to confirm wounding. We confirmed that this method reproducibly introduced bacteria into the wound using YFP-*S. aureus* (Figure S1A). CFUs present in the wound at a given timepoint was determined by taking a 2mm diameter ear punch and homogenizing the tissue in 1mL PBS. CFUs were determined by serial dilution and plating on TSB agar.

Author Manuscript Author Manuscript Author Manuscript Author Manuscript

Measurement of hla production in bacterial culture—WT *S. aureus* overnight culture was diluted 1:200 into fresh tryptic soy broth and grown with shaking at 37°C. Samples were taken every 30 min for 6 h for measurement of OD, CFU, and Hla concentration. Hla concentration was determined by sandwich ELISA using a monoclonal capture antibody (7B8) at 1 μg/ml[6], a rabbit polyclonal anti-Hla detection antibody[54] (1:2500), and HRP-conjugated goat anti-rabbit IgG (1:4000, Cell Signaling). The Hla concentration was calculated using a standard curve from recombinant Hla. These data were used to calculate approximate Hla production rates/10^8 CFU for bacteria at different stages of growth (Figure S4).

Estimation of hla content in experimental models

Ear scratch model: A 5μL drop containing ~1.5×10^9 CFU bacteria is applied to the ear and a scratch made through it with the needle. The droplet is then blotted off, thus the final CFU that is present in the wound is unknown, and likely somewhat variable. However, if somewhere between 10^5 and 10^7 bacteria are dispersed along the 100 μm × 2000 μm wound (we recover ~10^7 CFU in WT infection at 24h, Figure 7E), these bacteria could make ~0.35–35ng of Hla in an hour (based on our measurement of Hla production in bacterial cultures *in vitro*). The volume of distribution of this Hla is also unknown, however, since we see the effect of Hla on neutrophils within ~100μm of the wound edge, we assume that the Hla is primarily within this volume of $2 \times 10^7 \mu m^3$ = 0.02μL. Using this volume, this translates to an Hla concentration of 17–1700 μg/mL. The actual Hla production in tissue is likely much less in tissue compared to culture broth. Since we observe that most neutrophils are motile and alive, we expect that the actual Hla concentration is less than 50 μg/mL since above this concentration we and others[6] have observed neutrophil cell death.

***In vitro* clustering experiments:** The bacteria/agarose gel contains ~1.6×10^9 bacteria encased in a 200μL gel cast into a chamberslide. The neutrophils are added to the well within ~30–60 min. We estimate that this number of bacteria could produce up to ~5–6μg Hla/hour. This would equate to a concentration of ~28 μg/mL after 1 h. The Hla concentration at the gel edge (point of contact of neutrophils with gel) would be approximately equal to the gel concentration, then decrease at points further from the gel. This is consistent with our observation that the effect of the bacteria +/− toxin is most apparent immediately adjacent to the gel.

These estimates do not provide an exact measurement of Hla concentrations, and there are many unknowns, including how Hla production in the tissue compares to Hla production in broth. However, we can say that the concentrations of Hla (3–25 μg/mL) that produce a clear effect in our *in vitro* assays are within the range of expected Hla production *in vivo* based on number and growth phase of the bacteria.

Two-photon intravital microscopy—We used two different systems (*In Vivo* Imaging Core (IVIC) and Washington University Center for Cellular Imaging (WUCCI)) for imaging neutrophil behavior by intravital 2-photon microscopy. Results were similar in both systems. 1.5h after ear wounding, mice were anesthetized using isoflurane and stably positioned with the ear fixed on a custom-built, temperature-controlled mounting platforms.

Author Manuscript Author Manuscript Author Manuscript Author Manuscript

IVIC System: *In vivo* imaging was performed using a custom two-photon microscope built on an Olympus IX81 upright platform equipped with two Coherent Vision II T-Sapphire lasers, 4 PMT detectors (biand multi-alkali) and an 20x Olympus XLUMPLFLN 1.0 NA water dipping objective. Experiments used 900nm 2P excitation and emission was collected using 495nm, 540nm, 585nm dichroic filters (Semrock) to separate SHG(<495), GFP (495–540), YFP (540–585) and tdTomato (<580). Image acquisition was performed using SlideBook software (Intelligent Imaging Innovations). Time lapse recordings of 41 consecutive 2μm z-steps (512 × 512 pixels, 0.8 pixels/micron, 10f average/z) were acquired at 33 s intervals for 40 time points to document neutrophil motility, chemotaxis and clustering near the infected wound.

WUCCI System: Intravital microscopy was performed using an upright Nikon A1RHD25 MP multi-photon microscope. The system is also equipped with four non-descanned detectors (NDDs) for two-photon imaging in live animals. A Titanium Sapphire femtosecond infrared laser tuned to 920nm was used to excite eGFP and second harmonic generation (collagen). Images were acquired with a 25× water immersion objective (Numerical aperture 1.1, Nikon). Time lapse recordings of 20 consecutive 4μm z-steps (513 × 513 mm, 1024 × 1024 pixels) were acquired at 20–30 s intervals for 50 time points.

For analysis of all images, multi-dimensional image rendering, processing, analysis and cell tracking were performed using Imaris 9.8 (Bitplane, Zurich, Switzerland). Cell tracking data were analyzed using the Motility Lab online resource (2ptrack.net) that provide a user-friendly interface for cell migration analysis (https://doi.org/10.1016/j.immuno.2021.100003). Cluster size (green voxels) and distance from the wound were measured using FIJI Voxel Counter.

***In vivo* measurement of cytosolic calcium—**Two-photon microscopy images were collected using a customized dual Laser (InSight & Mai Tai both Spectra-Physics) Leica SP8 Upright Microscope equipped with a 25x and 0.95 numerical aperture water-immersion objective. Three channels were acquired simultaneous using a resonant scanner and lasers tuned to 910 and 985nm. Fluorescence emission was guided directly to external hybrid photodetectors (Leica). For signal separation, we used three separate dichroic beam splitters (without bandpass filters) FF640-FDi01, FF562-FDi03 and FF506-FDi03 (Semrock). The mirrors were arranged in dendritic fashion where settings generated four channels: approximately 390–506nm, 506–562nm, 562–640nm and 640–680nm (not recorded). For analysis, the cell surfaces were defined and the mean fluorescence intensities (green/GCamp6f and red/TdTomato) of the cell region were manually measured in ImageJ for all flashing cells within 150μm of the wound edge. The calcium spike amplitude was determined as $(green/red_{peak})/(green/red_{baseline})$. The spike duration was defined as the time during which calcium amplitude >1.1.

2D neutrophil chemotaxis assay—Bone marrow neutrophils were resuspended in an HBSS medium containing 2% fetal bovine serum, 20mM HEPES, 1mM $CaCl_2$ and 0.5mM $MgCl_2$ and seeded into the central channel (observation area) of Ibidi μ-Slides and incubated at 37°C in a humidified incubator for 30min to allow for cell adhesion. The two 60μL reservoirs connected by the central channel were filled with 65μL of the HBSS/

Author Manuscript Author Manuscript Author Manuscript Author Manuscript

HEPES/Ca/Mg medium and a chemokine gradient established by adding 30μL of 10 ng/mL C5a into the right reservoir with or without 3 or 6 μg/mL Hla. Neutrophil migration in the central channel was recorded by time-lapse brightfield microscopy (Zeiss AxioObserverZ.1 equipped with a Zeiss PLAN-ApoChromat 10× objective/Numerical aperture 0.45) every 30 s for 30min in a 37°C humidified chamber. In each chemotaxis experiment, ~30 motile cells (or 30 randomly selected tracks if few were motile) were tracked via Manual Tracking in ImageJ (NIH) and the migration tracks were analyzed by the Chemotaxis and Migration Tool (Ibidi).

***In vitro* clustering assay—**Ultrapure agarose powder was dissolved in PBS and cooled down to ~50°C in a water bath. 3mL of overnight culture of WT or *Δhla S. aureus* was centrifuged and pellets were resuspended in 100μL of PBS then added to the agarose solution at ratio of 1:50 (final 1% agarose, final CFU 1.6×10^9 per 200μL gel). The agarose/bacteria solution (200μL) was cast into one side of a cell chamber (Ibidi μ-Slide 8-well chamber slide) and allowed to solidify at room temperature for 10 min. Mouse bone marrow neutrophils were resuspended at 4×10^6/mL in HBSS containing 20mM HEPES, 1mM $CaCl_2$, 0.5mM $MgCl_2$ and 10% FBS. 20μL of the cell suspension was added to each cell chamber. In some experiments, DAPI was added to the cell suspension at final concentration of 2 μg/mL. After cells settled to the bottom of the chamber (about 5 min), neutrophil cluster formation was recorded using a Zeiss AxioObserverZ.1 (Zeiss PLAN-ApoChromat 10× objective, numerical aperture 0.45) microscope equipped with an environment chamber for live-cell imaging. Data acquisition was performed in both brightfield and DAPI channels (when applicable) every 1–2 min for 1h at 37°C. 1–2 fields per well were imaged. For analysis, the total number of clusters formed during the 1h imaging period and the duration of each cluster were manually counted. The size of each cluster was measured using Fuji/ImageJ (NIH). The number of DAPI-positive cells and total cell numbers in each field of view were counted manually at the final time point (1h) to determine the % DAPI+ cells.

Measurement of LTB4 production—Isolated bone marrow neutrophils were resuspended at 2×10^6/mL in HBSS containing 20mM HEPES, 1mM $CaCl_2$, 0.5mM $MgCl_2$ and stimulated in 96 well plates for 15 min with the indicated agonists. LTB4 was detected in the supernatents by competitive ELISA per the manufacturer's instructions (R&D).

Measurement of intracellular calcium levels—Intracellular calcium levels were measured by flow cytometry.[13] Isolated neutrophils or whole bone marrow were resuspended in HBSS/HEPES and loaded with 3μM Indo-1 a.m. and 2.5mM probenecid (Molecular Probes) at RT for 40 min. Cells were washed and resuspended in cold HBSS/H (2×10^7/mL), and bone marrow cells were blocked by anti-mouse CD16/CD32 (BD) and labeled with Ly-6G-BV785 (IA8; BD Pharmingen) and anti-mouse CD101-AF647 (BioLegend) for 40 min in the dark. For each run, cells (~5×10^5) were warmed to 37°C for 5 min, then run on the flow cytometer (LSRFortessa, BD) for 30 s to establish a baseline reading. Stimuli were added as indicated and the samples analyzed continuously. In experiments investigating the impact of Hla on neutrophil SOCE, stimuli were added first in a calcium-free media to observe intracellular calcium release, then 1mM of Ca^{2+} was added at 2 min to assess SOCE. Data were analyzed using FlowJo 9 software (Treestar). Calcium

Author Manuscript Author Manuscript Author Manuscript Author Manuscript

levels are expressed as relative ratios of fluorescence emission at 375nm/525nm (Indo-1 calcium bound/calcium unbound) and SOCE quantified as AUC of kinetic averages.

Measurement of membrane potential by flow cytometry—Isolated neutrophils or whole bone marrow labeled with Ly-6G and CD101 to identify mature neutrophils were resuspended in containing 20mM HEPES, 1mM $CaCl_2$, 0.5mM $MgCl_2$. ~5×10^5 cells were warmed incubated with 250nM DiBAC4(3) at 37°C for 8 min, then run on the flow cytometer (LSRFortessa, BD) for 30 s to establish a baseline reading. Stimuli were added as indicated and the samples continuously analyzed for change in fluorescence (FITC channel). Data were analyzed using FlowJo 9 software (Treestar). To allow comparison of relative changes in membrane potential across experiments, data are expressed as fold change in fluorescence over baseline. For experiments using sodium-free media, a sodium chloride or choline chloride-based media was used consisting of 140mM sodium/choline chloride, 4mM potassium chloride, 2.5mM glucose, 20mM HEPES, 1mM CaCl, 0.5mM MgCl, pH 7.4.

Measurement of cytosolic sodium—Isolated neutrophils were loaded with 5μM Na-green (Molecular Probes) and 2.5mM probenecid for 30 min at room temperature. Cells were then washed and resuspended in HBSS/HEPES/Ca/Mg and ~5×10^5 cells were warmed to 37°C then run on the flow cytometer (LSRFortessa, BD) for 30 s to establish a baseline reading. Stimuli were added as indicated and the samples analyzed continuously for change in fluorescence (FITC channel). Data were analyzed using FlowJo 9 software (Treestar). To allow comparison of relative changes in membrane potential across experiments, data are expressed as fold change in fluorescence over baseline.

***S. aureus* pneumonia model—**Following a 1:100 dilution of an overnight culture into fresh tryptic soy broth, WT or *Δhla S. aureus* was grown with shaking at 37°C to mid-log phase (OD 0.5 at 600 nm). 50mL culture aliquots were centrifuged and bacterial pellets were washed in PBS. Mice were anesthetized with ketamine (100 mg/kg) and xylazine (10 mg/kg) and 2.4×10^8 *S aureus* in 30 μL was administered by intranasal route. For bronchoalveolar lavage (BAL), mice were sacrificed using isoflurane and the trachea exposed by midline skin incision. A 20-gauge catheter was inserted into the trachea, followed by two washes of 1mL PBS containing 1mM EDTA. Retrieved lavage fluid from the first instillation was serially diluted for quantitative CFU analysis. Recovered lavage fluid from the two instillations were combined, spun down, and stained for Ly6G and CD11b to identify BAL neutrophils. Total cell count and neutrophil count were analyzed by flow cytometry. For counting whole lung CFUs, mice were sacrificed by high dose isoflurane and lungs were perfused with 10mL PBS injected through the right ventricle. The lung then was surgically excised and minced. The pieces were digested in HBSS containing 2% FBS, 20mM HEPES, 2.2 Wünsch U/mL collagenase D, and 50U/mL DNase in a shaker at 37°C for 45 min 0.1M EDTA was added to the lung digestion for 5 min additional incubation to inactivate the collagenase. The lung pieces were poured through a 70mm cell strainer and the digested lung samples serially diluted for quantitative CFU analysis.

Author Manuscript Author Manuscript Author Manuscript Author Manuscript

QUANTIFICATION AND STATISTICAL ANALYSIS

Data shown are expressed as mean ± SD unless otherwise indicated. Where possible the individual data points are graphed. The data represented by each point and the number of experiments represented is defined in the figure legends. Data were graphed using Prism GraphPad software and figures prepared using Adobe Illustrator (software licensed to Washington University). Groups were compared using unpaired 2-tailed Student's t test (for normal distribution), Mann-Whitney-U test (nonnormal distribution) or repeated-measures analysis of variance (ANOVA) as indicated in the figure legends. For experiments with large inter-experiment variability in WT neutrophil response, data from independent experiments was combined by normalizing to WT for each experiment. Statistical significance for these experiments was determined using a one sample t test compared to a theoretical value of 1. $p < 0.05$ was considered to be significant.

Supplementary Material

Refer to Web version on PubMed Central for supplementary material.

ACKNOWLEDGMENTS

2P-IVM was performed in part through the use of Washington University Center for Cellular Imaging (WUCCI) supported by the Washington University School of Medicine, The Children's Discovery Institute of Washington University, St. Louis Children's Hospital (CDI-CORE-2015–505 and CDI-CORE-2019–813), and the Foundation for Barnes-Jewish Hospital (3770 and 4642), as well as Seonyoung Kim and the Washington University In Vivo Imaging Core. We would like to thank Reuben Olaniyi for construction of the *hla*-deletion USA300/LAC *S. aureus* strain. This work was supported by NIH grant R01AI166793 (R.A.C.). Additional support was supplied by R37AI04953 to G.J.R and R01AI097434 to J.B.W.

INCLUSION AND DIVERSITY

We support inclusive, diverse, and equitable conduct of research.

REFERENCES

1. Guerra FE, Borgogna TR, Patel DM, Sward EW, and Voyich JM (2017). Epic Immune Battles of History: Neutrophils vs. Staphylococcus aureus. Front. Cell. Infect. Microbiol. 7, 286. 10.3389/fcimb.2017.00286. [PubMed: 28713774]
2. Berube BJ, and Bubeck Wardenburg J (2013). Staphylococcus aureus alpha-toxin: nearly a century of intrigue. Toxins 5, 1140–1166. 10.3390/toxins5061140. [PubMed: 23888516]
3. Wilke GA, and Bubeck Wardenburg J (2010). Role of a disintegrin and metalloprotease 10 in Staphylococcus aureus alpha-hemolysin-mediated cellular injury. Proc. Natl. Acad. Sci. USA 107, 13473–13478. 10.1073/pnas.1001815107. [PubMed: 20624979]
4. Berube BJ, Sampedro GR, Otto M, and Bubeck Wardenburg J (2014). The psmalpha locus regulates production of Staphylococcus aureus alpha-toxin during infection. Infect. Immun. 82, 3350–3358. 10.1128/IAI.00089-14. [PubMed: 24866799]
5. Powers ME, Becker REN, Sailer A, Turner JR, and Bubeck Wardenburg J (2015). Synergistic Action of Staphylococcus aureus alphaToxin on Platelets and Myeloid Lineage Cells Contributes to Lethal Sepsis. Cell Host Microbe 17, 775–787. 10.1016/j.chom.2015.05.011. [PubMed: 26067604]
6. Becker REN, Berube BJ, Sampedro GR, DeDent AC, and Bubeck Wardenburg J (2014). Tissue-specific patterning of host innate immune responses by Staphylococcus aureus alpha-toxin. J. Innate Immun. 6, 619–631. 10.1159/000360006. [PubMed: 24820433]

Author Manuscript Author Manuscript Author Manuscript Author Manuscript

7. Song L, Hobaugh MR, Shustak C, Cheley S, Bayley H, and Gouaux JE (1996). Structure of staphylococcal alpha-hemolysin, a heptameric transmembrane pore. Science 274, 1859–1866. 10.1126/science.274.5294.1859. [PubMed: 8943190]

8. von Hoven G, Qin Q, Neukirch C, Husmann M, and Hellmann N (2019). Staphylococcus aureus alpha-toxin: small pore, large consequences. Biol. Chem. 400, 1261–1276. 10.1515/hsz-2018-0472. [PubMed: 30951494]

9. Boucek MM, and Snyderman R (1976). Calcium influx requirement for human neutrophil chemotaxis: inhibition by lanthanum chloride. Science 193, 905–907. [PubMed: 948752]

10. Korchak HM, Rutherford LE, and Weissmann G (1984). Stimulus response coupling in the human neutrophil. I. Kinetic analysis of changes in calcium permeability. J. Biol. Chem. 259, 4070–4075. [PubMed: 6323454]

11. Clemens RA, and Lowell CA (2019). CRAC channel regulation of innate immune cells in health and disease. Cell Calcium 78, 56–65. 10.1016/j.ceca.2019.01.003. [PubMed: 30641250]

12. Zhang H, Clemens RA, Liu F, Hu Y, Baba Y, Theodore P, Kurosaki T, and Lowell CA (2014). STIM1 calcium sensor is required for activation of the phagocyte oxidase during inflammation and host defense. Blood 123, 2238–2249. 10.1182/blood-2012-08-450403. [PubMed: 24493668]

13. Grimes D, Johnson R, Pashos M, Cummings C, Kang C, Sampedro GR, Tycksen E, McBride HJ, Sah R, Lowell CA, and Clemens RA (2020). ORAI1 and ORAI2 modulate murine neutrophil calcium signaling, cellular activation, and host defense. Proc. Natl. Acad. Sci. USA 117, 24403–24414. 10.1073/pnas.2008032117. [PubMed: 32929002]

14. Suttorp N, Seeger W, Zucker-Reimann J, Roka L, and Bhakdi S (1987). Mechanism of leukotriene generation in polymorphonuclear leukocytes by staphylococcal alpha-toxin. Infect. Immun. 55, 104–110. 10.1128/iai.55.1.104-110.1987. [PubMed: 3025097]

15. Suttorp N, and Habben E (1988). Effect of staphylococcal alpha-toxin on intracellular Ca2+ in polymorphonuclear leukocytes. Infect. Immun. 56, 2228–2234. 10.1128/iai.56.9.2228-2234.1988. [PubMed: 3137163]

16. Gemmell CG, Peterson PK, Schmeling DJ, and Quie PG (1982). Effect of staphylococcal alpha-toxin on phagocytosis of staphylococci by human polymorphonuclear leukocytes. Infect. Immun. 38, 975–980. 10.1128/iai.38.3.975-980.1982. [PubMed: 7152682]

17. Schmeling DJ, Gemmell CG, Craddock PR, Quie PG, and Peterson PK (1981). Effect of staphylococcal alpha-toxin on neutrophil migration and adhesiveness. Inflammation 5, 313–322. 10.1007/BF00911095. [PubMed: 7327697]

18. Tkaczyk C, Hamilton MM, Datta V, Yang XP, Hilliard JJ, Stephens GL, Sadowska A, Hua L, O'Day T, Suzich J, et al. (2013). Staphylococcus aureus alpha toxin suppresses effective innate and adaptive immune responses in a murine dermonecrosis model. PLoS One 8, e75103. 10.1371/journal.pone.0075103. [PubMed: 24098366]

19. Bartlett AH, Foster TJ, Hayashida A, and Park PW (2008). Alpha-toxin facilitates the generation of CXC chemokine gradients and stimulates neutrophil homing in Staphylococcus aureus pneumonia. J. Infect. Dis. 198, 1529–1535. 10.1086/592758. [PubMed: 18823272]

20. Faust N, Varas F, Kelly LM, Heck S, and Graf T (2000). Insertion of enhanced green fluorescent protein into the lysozyme gene creates mice with green fluorescent granulocytes and macrophages. Blood 96, 719–726. [PubMed: 10887140]

21. Abram CL, Roberge GL, Hu Y, and Lowell CA (2014). Comparative analysis of the efficiency and specificity of myeloid-Cre deleting strains using ROSA-EYFP reporter mice. J. Immunol. Methods 408, 89–100. 10.1016/j.jim.2014.05.009. [PubMed: 24857755]

22. Henke MO, Renner A, Rubin BK, Gyves JI, Lorenz E, and Koo JS(2006). Up-regulation of S100A8 and S100A9 protein in bronchial epithelial cells by lipopolysaccharide. Exp. Lung Res. 32, 331–347. 10.1080/01902140600959580. [PubMed: 17090475]

23. Mørk G, Schjerven H, Mangschau L, Søyland E, and Brandtzaeg P (2003). Proinflammatory cytokines upregulate expression of calprotectin (L1 protein, MRP-8/MRP-14) in cultured human keratinocytes. Br. J. Dermatol. 149, 484–491. 10.1046/j.1365-2133.2003.05536.x. [PubMed: 14510979]

24. Fujita Y, Khateb A, Li Y, Tinoco R, Zhang T, Bar-Yoseph H, Tam MA, Chowers Y, Sabo E, Gerassy-Vainberg S, et al. (2018). Regulation of S100A8 Stability by RNF5 in Intestinal Epithelial

Author Manuscript Author Manuscript Author Manuscript Author Manuscript

Cells Determines Intestinal Inflammation and Severity of Colitis. Cell Rep. 24, 3296–3311.e6. 10.1016/j.celrep.2018.08.057. [PubMed: 30232010]

25. Weber S, Niessen MT, Prox J, Lullmann-Rauch R, Schmitz A,€ Schwanbeck R, Blobel CP, Jorissen E, de Strooper B, Niessen CM, and Saftig P. (2011). The disintegrin/metalloproteinase Adam10 is essential for epidermal integrity and Notch-mediated signaling. Development 138, 495–505. 10.1242/dev.055210. [PubMed: 21205794]
26. Lämmermann T, Afonso PV, Angermann BR, Wang JM, Kastenmüller W, Parent CA, and Germain RN (2013). Neutrophil swarms require LTB4 and integrins at sites of cell death in vivo. Nature 498, 371–375. 10.1038/nature12175. [PubMed: 23708969]
27. Lee EKS, Gillrie MR, Li L, Arnason JW, Kim JH, Babes L, Lou Y, Sanati-Nezhad A, Kyei SK, Kelly MM, et al. (2018). Leukotriene B4-Mediated Neutrophil Recruitment Causes Pulmonary Capillaritis during Lethal Fungal Sepsis. Cell Host Microbe 23, 121–133.e4. 10.1016/j.chom.2017.11.009. [PubMed: 29290576]
28. Jover E, Tawk MY, Laventie BJ, Poulain B, and Prévost G (2013). Staphylococcal leukotoxins trigger free intracellular Ca(2+) rise in neurones, signalling through acidic stores and activation of store-operated channels. Cell Microbiol. 15, 742–758. 10.1111/cmi.12069. [PubMed: 23152983]
29. Reich EP, Cui L, Yang L, Pugliese-Sivo C, Golovko A, Petro M, Vassileva G, Chu I, Nomeir AA, Zhang LK, et al. (2005). Blocking ion channel KCNN4 alleviates the symptoms of experimental autoimmune encephalomyelitis in mice. Eur. J. Immunol. 35, 1027–1036. 10.1002/eji.200425954. [PubMed: 15770697]
30. Chiang EY, Li T, Jeet S, Peng I, Zhang J, Lee WP, DeVoss J, Caplazi P, Chen J, Warming S, et al. (2017). Potassium channels Kv1.3 and KCa3.1 cooperatively and compensatorily regulate antigen-specific memory T cell functions. Nat. Commun. 8, 14644. 10.1038/ncomms14644. [PubMed: 28248292]
31. Dong TX, Othy S, Jairaman A, Skupsky J, Zavala A, Parker I, Dynes JL, and Cahalan MD (2017). T-cell calcium dynamics visualized in a ratiometric tdTomato-GCaMP6f transgenic reporter mouse. Elife 6, e32417. 10.7554/eLife.32417. [PubMed: 29239725]
32. Orthgiess J, Gericke M, Immig K, Schulz A, Hirrlinger J, Bechmann I, and Eilers J (2016). Neurons exhibit Lyz2 promoter activity in vivo: Implications for using LysM-Cre mice in myeloid cell research. Eur. J. Immunol. 46, 1529–1532. 10.1002/eji.201546108. [PubMed: 27062494]
33. Klein EY, Mojica N, Jiang W, Cosgrove SE, Septimus E, Morgan DJ, and Laxminarayan R (2017). Trends in Methicillin-Resistant Staphylococcus aureus Hospitalizations in the United States, 2010–2014. Clin. Infect. Dis. 65, 1921–1923. 10.1093/cid/cix640. [PubMed: 29020322]
34. Kwiecinski JM, Kratofil RM, Parlet CP, Surewaard BGJ, Kubes P, and Horswill AR (2021). Staphylococcus aureus uses the ArlRS and MgrA cascade to regulate immune evasion during skin infection. Cell Rep. 36, 109462. 10.1016/j.celrep.2021.109462. [PubMed: 34320352]
35. Liese J, Rooijakkers SHM, van Strijp JAG, Novick RP, and Dustin ML (2013). Intravital two-photon microscopy of host-pathogen interactions in a mouse model of Staphylococcus aureus skin abscess formation. Cell Microbiol. 15, 891–909. 10.1111/cmi.12085. [PubMed: 23217115]
36. Yang C, Ruiz-Rosado J.d.D., Robledo-Avila FH, Li Z, Jennings RN, Partida-Sanchez S, and Montgomery CP. (2021). Antibody-Mediated Protection against Staphylococcus aureus Dermonecrosis: Synergy of Toxin Neutralization and Neutrophil Recruitment. J. Invest. Dermatol. 141, 810–820.e8. 10.1016/j.jid.2020.09.001. [PubMed: 32946878]
37. Abtin A, Jain R, Mitchell AJ, Roediger B, Brzoska AJ, Tikoo S, Cheng Q, Ng LG, Cavanagh LL, von Andrian UH, et al. (2014). Perivascular macrophages mediate neutrophil recruitment during bacterial skin infection. Nat. Immunol. 15, 45–53. 10.1038/ni.2769. [PubMed: 24270515]
38. Tam K, and Torres VJ (2019). Staphylococcus aureus Secreted Toxins and Extracellular Enzymes. Microbiol. Spectr. 7. 10.1128/microbiolspec.GPP3-0039-2018.
39. Seiß EA, Krone A, Formaglio P, Goldmann O, Engelmann S, Schraven B, Medina E, and Müller AJ (2019). Longitudinal proliferation mapping in vivo reveals NADPH oxidase-mediated dampening of Staphylococcus aureus growth rates within neutrophils. Sci. Rep. 9, 5703. 10.1038/s41598-019-42129-6. [PubMed: 30952906]

Author Manuscript Author Manuscript Author Manuscript Author Manuscript

40. Clemens RA, Chong J, Grimes D, Hu Y, and Lowell CA (2017). STIM1 and STIM2 cooperatively regulate mouse neutrophil store-operated calcium entry and cytokine production. Blood 130, 1565–1577. 10.1182/blood-2016-11-751230. [PubMed: 28724541]
41. Chauhan A, Sun Y, Pani B, Quenumzangbe F, Sharma J, Singh BB, and Mishra BB (2014). Helminth induced suppression of macrophage activation is correlated with inhibition of calcium channel activity. PLoS One 9, e101023. 10.1371/journal.pone.0101023. [PubMed: 25013939]
42. Dellis O, Arbabian A, Papp B, Rowe M, Joab I, and Chomienne C (2011). Epstein-Barr virus latent membrane protein 1 increases calcium influx through store-operated channels in B lymphoid cells. J. Biol. Chem. 286, 18583–18592. 10.1074/jbc.M111.222257. [PubMed: 21454636]
43. Hyser JM, Utama B, Crawford SE, Broughman JR, and Estes MK (2013). Activation of the endoplasmic reticulum calcium sensor STIM1 and store-operated calcium entry by rotavirus requires NSP4 viroporin activity. J. Virol. 87, 13579–13588. 10.1128/JVI.02629-13. [PubMed: 24109210]
44. Khazen R, Corre B, Garcia Z, Lemaître F, Bachellier-Bassi S, d'Enfert C, and Bousso P (2022). Spatiotemporal dynamics of calcium signals during neutrophil cluster formation. Proc. Natl. Acad. Sci. USA 119, e2203855119. 10.1073/pnas.2203855119. [PubMed: 35858359]
45. Steinckwich N, Myers P, Janardhan KS, Flagler ND, King D, Petranka JG, and Putney JW (2015). Role of the store-operated calcium entry protein, STIM1, in neutrophil chemotaxis and infiltration into a murine model of psoriasis-inflamed skin. Faseb. J. : official publication of the Federation of American Societies for Experimental Biology 29, 3003–3013. 10.1096/fj.14-265215.
46. Inoshima I, Inoshima N, Wilke GA, Powers ME, Frank KM, Wang Y, and Bubeck Wardenburg J (2011). A Staphylococcus aureus poreforming toxin subverts the activity of ADAM10 to cause lethal infection in mice. Nat. Med. 17, 1310–1314. 10.1038/nm.2451. [PubMed: 21926978]
47. Spaan AN, van Strijp JAG, and Torres VJ (2017). Leukocidins: staphylococcal bi-component pore-forming toxins find their receptors. Nat. Rev. Microbiol. 15, 435–447. 10.1038/nrmicro.2017.27. [PubMed: 28420883]
48. Nauseef WM (2023). Human neutrophils not equal murine neutrophils: Does it matter? Immunol. Rev. 314, 442–456. 10.1111/imr.13154. [PubMed: 36380497]
49. Medetgul-Ernar K, and Davis MM (2022). Standing on the shoulders of mice. Immunity 55, 1343–1353. 10.1016/j.immuni.2022.07.008. [PubMed: 35947979]
50. Baba Y, Nishida K, Fujii Y, Hirano T, Hikida M, and Kurosaki T (2008). Essential function for the calcium sensor STIM1 in mast cell activation and anaphylactic responses. Nat Immunol. 9, 81–88. [PubMed: 18059272]
51. Matsumoto M, Fujii Y, Baba A, Hikida M, Kurosaki T, and Baba Y (2011). The calcium sensors STIM1 and STIM2 control B cell regulatory function through interleukin-10 production. Immunity. 34, 703–714. [PubMed: 21530328]
52. Bubeck Wardenburg J, Bae T, Otto M, Deleo FR, and Schneewind O (2007). Poring over pores: alpha-hemolysin and Panton-Valentine leukocidin in Staphylococcus aureus pneumonia. Nat. Med. 13, 1405–1406. 10.1038/nm1207-1405. [PubMed: 18064027]
53. Bose JL, Fey PD, and Bayles KW (2013). Genetic tools to enhance the study of gene function and regulation in Staphylococcus aureus. Appl. Environ. Microbiol. 79, 2218–2224. 10.1128/AEM.00136-13. [PubMed: 23354696]
54. Bubeck Wardenburg J, and Schneewind O (2008). Vaccine protection against Staphylococcus aureus pneumonia. J. Exp. Med. 205, 287–294. 10.1084/jem.20072208. [PubMed: 18268041]

Author Manuscript Author Manuscript Author Manuscript Author Manuscript

Highlights

- *S. aureus* α-toxin disrupts the cell membrane potential to impair neutrophil SOCE
- *S. aureus* α-toxin impairs neutrophil localization and clustering at sites of infection
- Neutrophil mis-localization correlates with impaired bacterial control

Author Manuscript Author Manuscript Author Manuscript Author Manuscript

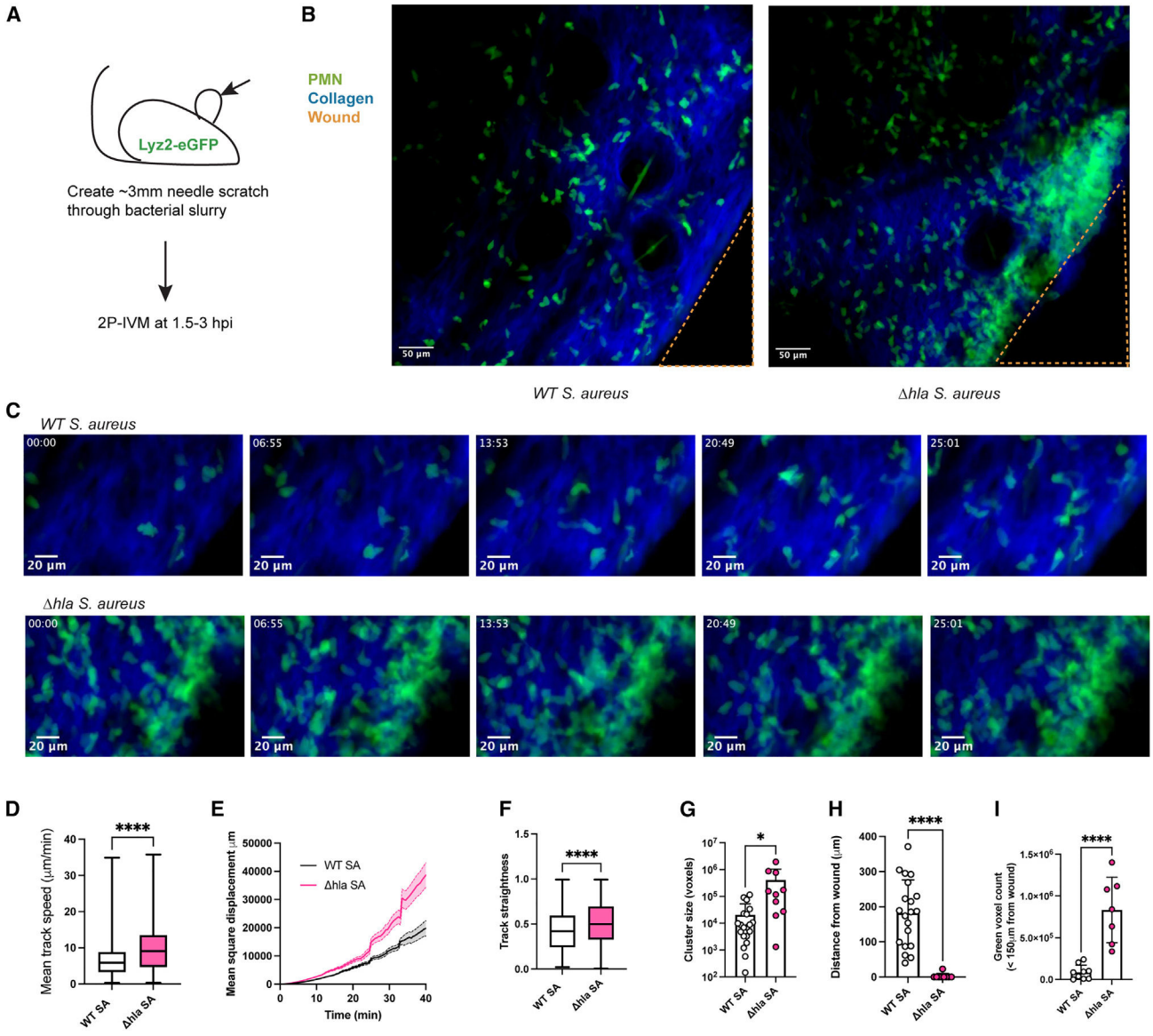

Figure 1. Hla disrupts early neutrophil migration and clustering in *S. aureus* infection

(A) A small superficial needle scratch was infected with WT or Δhla S. aureus (SA) on the pinnae of *Lyz2-EGFP* mice. The pattern of the early neutrophil response (1.5–3 hpi) was recorded by intravital 2-photon microscopy (2P-IVM), showing EGFP-neutrophils (green) and collagen-SHG (blue).

(B) Representative 2P fluorescence images of neutrophil migration and clustering at WT (left) or *Δhla* SA (right) wounds. The location of the wound is indicated by the dashed lines. Scale bar = 50 μm.

(C) Time course fluorescence images showing neutrophil accumulation at the wound in WT (top) vs. *Δhla* (bottom) SA infection. Scale bar = 20 μm.

(D–F) Plots of neutrophil mean track speed, square displacement, and track straightness in WT or *Δhla* SA infection. ~1,000 individual cells from 3–4 independent experiments per genotype were manually tracked using Imaris, and track data were plotted in MotilityLab.

Author Manuscript Author Manuscript Author Manuscript Author Manuscript

(G and H) Size (green voxels) and distance from the wound of neutrophil clusters formed in WT or *Δhla* SA infection. Each dot represents a cluster. Clusters (size and distance) were analyzed in 8–10 images from 4–5 independent experiments per genotype.
(I) Neutrophil quantity (green voxels) formed within 150 μm WT or *Δhla* SA infection site. Each dot represents the quantified voxels within 150 μm of the wound from one image. n = 8–10 images from 4–5 independent experiments per genotype. Unpaired t test. *p < 0.05; **p < 0.01; ***p < 0.001; ****p < 0.0001. Box and whisker plots (D, F) show median, quartiles 1–3 (boxes), and min-max (whiskers). Error bars represent standard deviation. SHG, second-harmonic generation.

Author Manuscript
Author Manuscript
Author Manuscript
Author Manuscript

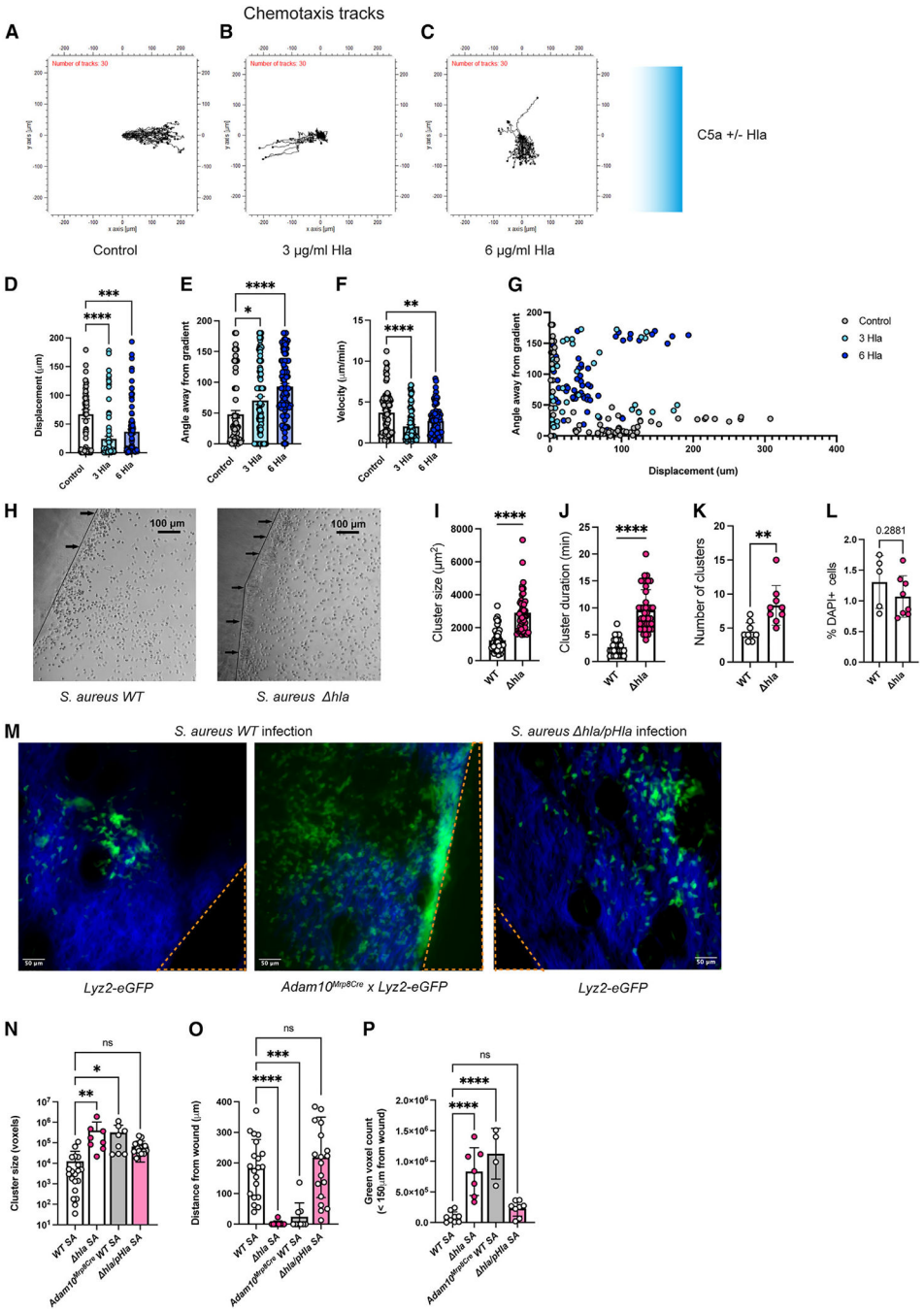

Figure 2. Hla directly impairs neutrophil chemotaxis and clustering

(A–C) Representative cell chemotaxis tracks of neutrophils migrating toward 10 ng/mL C5a with or without the indicated concentrations of Hla as shown by the blue gradient. The first point of each track was normalized to x = 0 and y = 0.

(D–F) Neutrophil chemotaxis parameters, displacement (D), angle away from the gradient (E), and velocity (F), analyzed by the Ibidi Chemotaxis and Migration Tool. Data represent ~100 cells per condition tracked from 3–4 independent experiments.

Author Manuscript Author Manuscript Author Manuscript Author Manuscript

(G) Scatterplot of the angle parameter against cell displacement. Each dot represents one cell.
(H) Representative bright-field images of neutrophil cluster formation (arrows) with exposure to WT (left) or *Δhla* (right) SA embedded in agarose gel. Scale bar = 100 μm.
(I–K) Quantitation of cluster size (I), duration (J), and number (K). For (I) and (J), each dot represents one cluster. For (K), each dot represents one experiment. Clusters were counted over the 1 h time-lapse video and combined from 6 independent experiments.
(L) In some experiments, DAPI was added to the media to identify dead/dying cells. Data represent the percentage of DAPI+ cells in each field of view at 1 h from 3 independent experiments.
(M) Representative fluorescence images from WT SA infection in *Lyz2-EGFP* (left), *Lyz2-EGFP* × *Adam10*^{MRP8Cre} (middle), or complemented *Δhla/phla* SA infection in *Lyz2-EGFP* mice (right) showing EGFP-neutrophils (green) and collagen/SHG (blue). Scale bar: 50 μm. Wound is indicated by the dotted line. Scale bar = 50 μm.
(N–P) Quantitation of cluster size (voxels), cluster distance from wound (O), and volume (voxels) of neutrophils within 150 μm of the wound edge (P). Note: in (N)–(P), the cumulative imaging data from WT mice are replicated from Figure 1 to facilitate comparison with *Adam10*^{MRP8Cre} mice and complemented *Δhla/phla* SA infection. Data points in (N)–(O) represent individual clusters counted from 4–10 images from 2–5 independent experiments. Data points in (P) represent individual images from 2–5 independent experiments.
(D–F) One-way ANOVA. (I–L) Student's unpaired t test. (N–P) One-way ANOVA. *$p < 0.05$; **$p < 0.01$; ***$p < 0.001$; ****$p < 0.0001$. ns, no significance; Error bars represent standard deviation. SA, *S. aureus*. SHG, second-harmonic generation.

Author Manuscript Author Manuscript Author Manuscript Author Manuscript

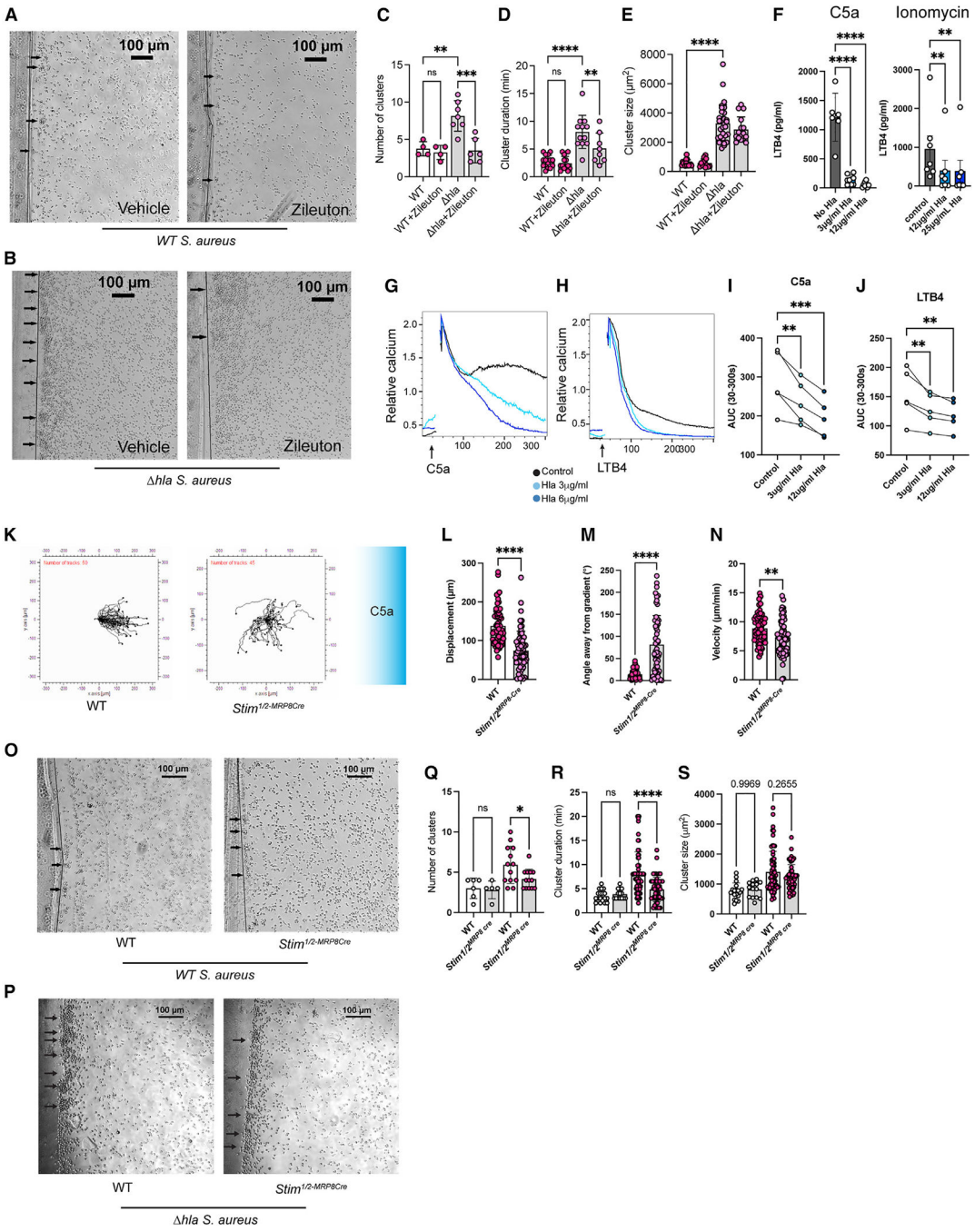

Figure 3. Hla disrupts neutrophil production of LTB4

(A and B) Representative bright-field images of neutrophil cluster formation with exposure to WT (A) or *Δhla* (B) SA embedded in agarose gel ± 10 mm Zileuton. Scale bar = 100 μm. (C–E) Quantitation of cluster number (C), duration (D), and size (E). For (C), each dot represents one experiment. For (D) and (E), each dot represents one cluster. Clusters were counted over the 1 h time-lapse video and combined from 6 independent experiments. (F) LTB4 production by bone marrow neutrophils stimulated for 15 min with C5a (10 ng/mL) or ionomycin (100 nM) in the presence of the indicated concentration of Hla.

Author Manuscript Author Manuscript Author Manuscript Author Manuscript

(G and H) Calcium influx in neutrophils stimulated with C5a or LTB4 in the presence of the indicated concentration of Hla was measured by flow cytometry.

(I and J) Quantitation of area under the curve (AUC) of calcium tracings from 5 independent experiments. Matched data from individual experiments are shown due to day-to-day variability in calcium response.

(K) Representative cell chemotaxis tracks of WT (left) and *Stim1/2*^{MRP8Cre} (right) neutrophils migrating toward 10 ng/mL C5a as shown by the blue gradient. The first point of each track was normalized to x = 0 and y = 0.

(L–N) Neutrophil chemotaxis parameters, displacement (L), angle away from the gradient (M), and velocity (N), analyzed by the Ibidi Chemotaxis and Migration Tool. Each dot represents one cell. Data in (L)–(N) represent ~100 cells per condition tracked from 3–4 independent experiments.

(O and P) Representative bright-field images of WT (left) and *Stim1/2*^{MRP8Cre} (right) neutrophil cluster formation with exposure to WT (O) or *Δhla* (P) SA embedded in agarose gel. Scale bar = 100 μm.

(Q–S) Quantitation of number, duration, and size of clusters from (O) and (P), from 3 independent experiments.

(C–E and P–R) Unpaired t test. (F) One way ANOVA. (I and J) One-way ANOVA with matching. *p < 0.05; **p < 0.01; ***p < 0.001; ****p < 0.0001. Error bars represent standard deviation.

Author Manuscript Author Manuscript Author Manuscript Author Manuscript

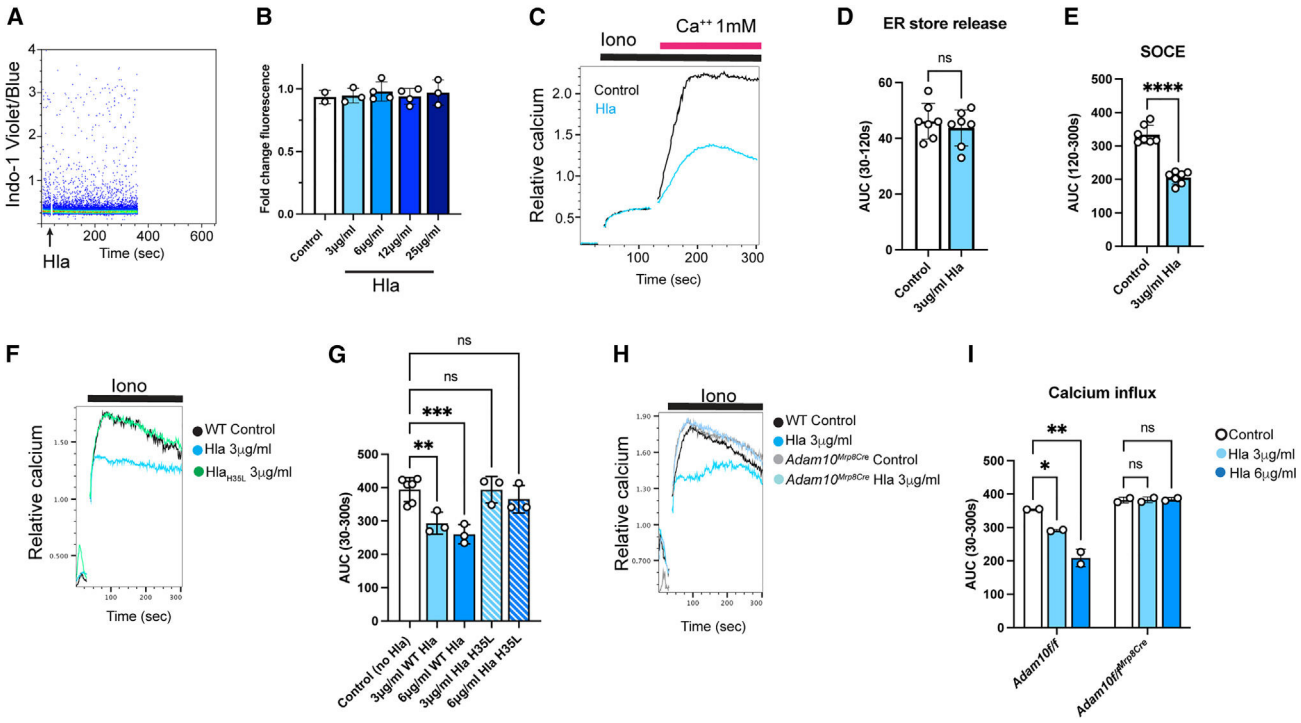

Figure 4. Hla inhibits neutrophil SOCE

(A) Representative plot showing calcium levels in neutrophils at baseline and after application of Hla (see arrow).

(B) Fold change in fluorescent ratio (indo-1 violet/blue) at 6 min vs. baseline in neutrophils exposed to the indicated concentrations of Hla.

(C) SOCE in neutrophils was measured by flow cytometry. Cells were stimulated by ionomycin (100 nM) to induce ER calcium release followed by addition of calcium to the media to measure calcium influx through plasma membrane CRAC channels. Where indicated, neutrophils were pre-treated for 5 min with 3 μg/mL Hla.

(D and E) Quantitation of AUC for 30–120 (ER calcium release) and 120–300 s (SOCE). Data are representative of 7 biological replicates from 4–5 independent experiments.

(F) Representative calcium tracings from neutrophils stimulated by ionomycin in cells pre-treated with vehicle, Hla, or the pore-forming mutant Hla_{H35L}.

(G) Quantitation of calcium entry (AUC) from data combined from 3–5 independent experiments.

(H) Representative calcium tracings from neutrophils stimulated by ionomycin in WT or *Adam10*^{MRP8Cre} neutrophils pre-treated with or without Hla.

(I) Quantitation of calcium entry (AUC) from data combined from 2 independent experiments.

(B) One-way ANOVA. (D and E) Student's t test. (H) Multiple t tests. (I) Two-way ANOVA. *p < 0.05; **p < 0.01; ***p < 0.001; ****p < 0.0001. Error bars represent standard deviation.

Author Manuscript Author Manuscript Author Manuscript Author Manuscript

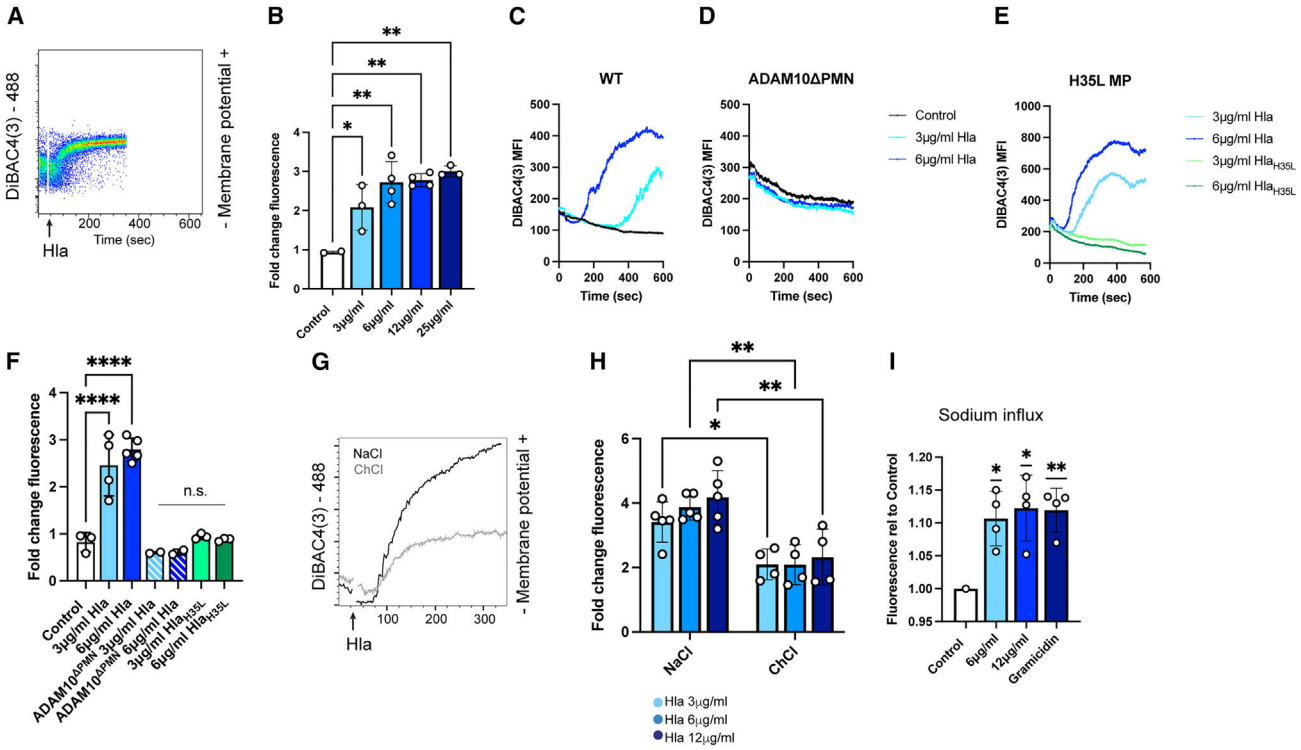

Figure 5. Ion flux through Hla pore depolarizes the neutrophil membrane potential

(A) Representative plot showing change in fluorescence of the membrane-potential-sensitive dye DIBAC4(3) in neutrophils at baseline and after application of Hla (see arrow).

(B) Fold change in DIBAC4(3) fluorescence at 6 min vs. baseline in neutrophils exposed to the indicated concentrations of Hla.

(C–E) Representative tracings of DIBAC4(3) MFI after application of Hla in WT (C) or *Adam10*^{MRP8Cre} (D) neutrophils or in WT neutrophils after application of the pore mutant Hla_{H35L} (E).

(F) Quantitation of (C)–(E) showing fold change in DIBAC4(3) MFI at 6 min vs. baseline from data compiled from 2–5 independent experiments.

(G) Representative tracing showing change in fluorescence of the membrane-potential-sensitive dye DIBAC4(3) in neutrophils after application of Hla in eitherNa+-containing or Na+-substitution media (choline chloride).

(H) Quantitation of (G) showing fold change in DIBAC4(3) MFI at 6 min vs. baseline from data compiled from 4 independent experiments.

(I) Sodium influx after addition of the indicated concentration of Hla was measured using the sodium indicator Na Green-AM. Data show the fluorescence at 6 minrelative to control.

(B) One-way ANOVA. (F) Multiple t tests. (H) Two-way ANOVA. (I) One-way ANOVA. *p < 0.05; **p < 0.01; ***p < 0.001; ****p < 0.0001. Error bars represent standard deviation.

Author Manuscript Author Manuscript Author Manuscript Author Manuscript

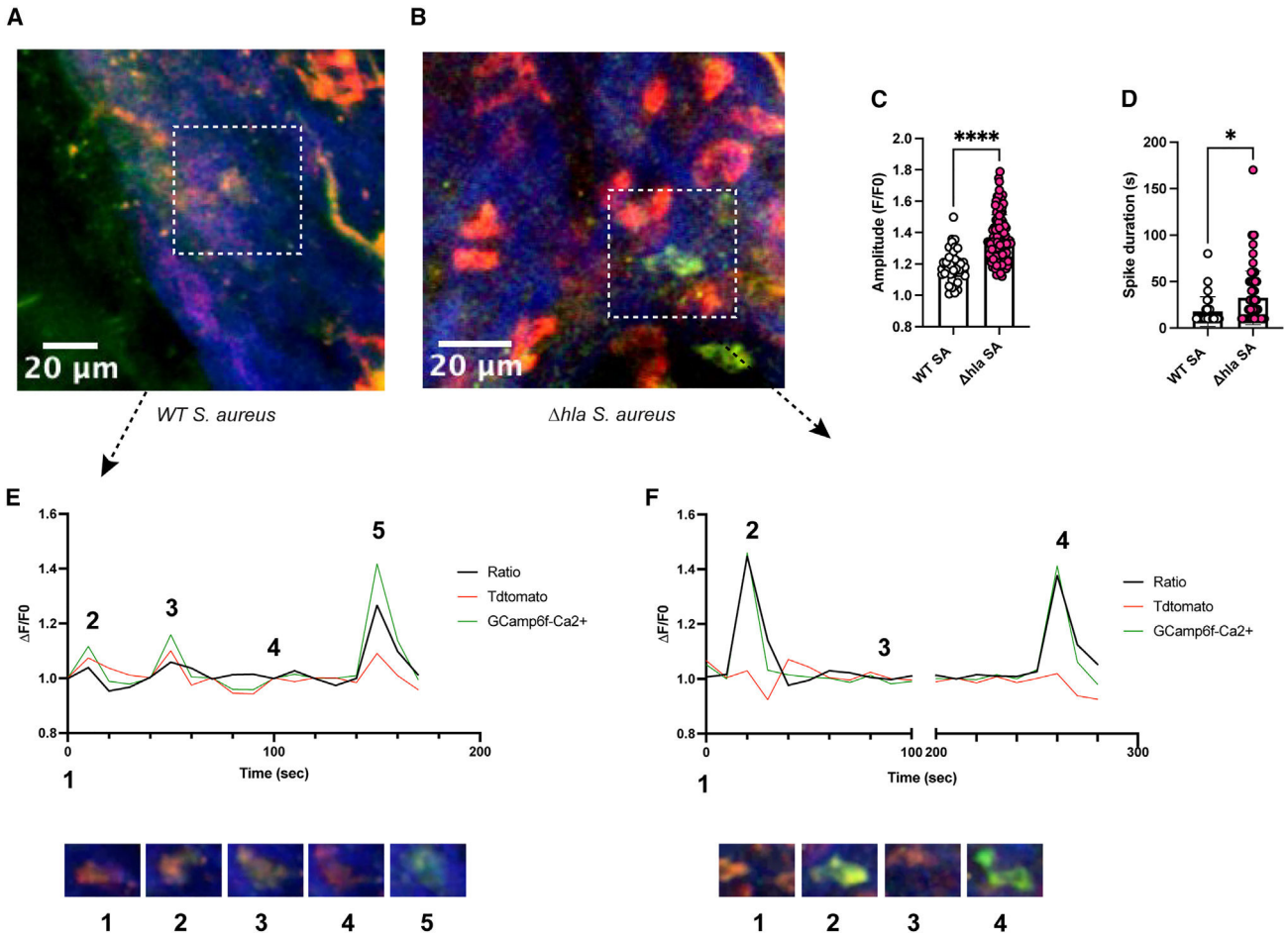

Figure 6. Hla disrupts neutrophil calcium signaling *in vivo*

(A and B) Representative fluorescence images of calcium signals during *WT* (A) and *Δhla* (B) SA infection. Scale bar = 20 μm.

(C and D) Quantitation of calcium spike amplitude and duration. For each cell, the ratio of the GCaMP6f (green-calcium)/TdTomato (red) signal was calculated, and data are expressed as $ratio_{peak}/ratio_{baseline}$ (F/F_0). Spike duration was determined as time F/F_0 >1.1. Data are representative of >100 cells compiled from 4–5 independent experiments.

(E and F) Representative tracing of TdTomato (red), GCamp6f (green), and TdTomato/GCamp6f ratio and the associated image of calcium signal from a single cell from WT (E) or *Δhla* (F) SA infection.

(C) Student's t test. (D) Mann-Whitney U test. *p < 0.05; **p < 0.01; ***p < 0.001; ****p < 0.0001. Error bars represent standard deviation.

Author Manuscript Author Manuscript Author Manuscript Author Manuscript

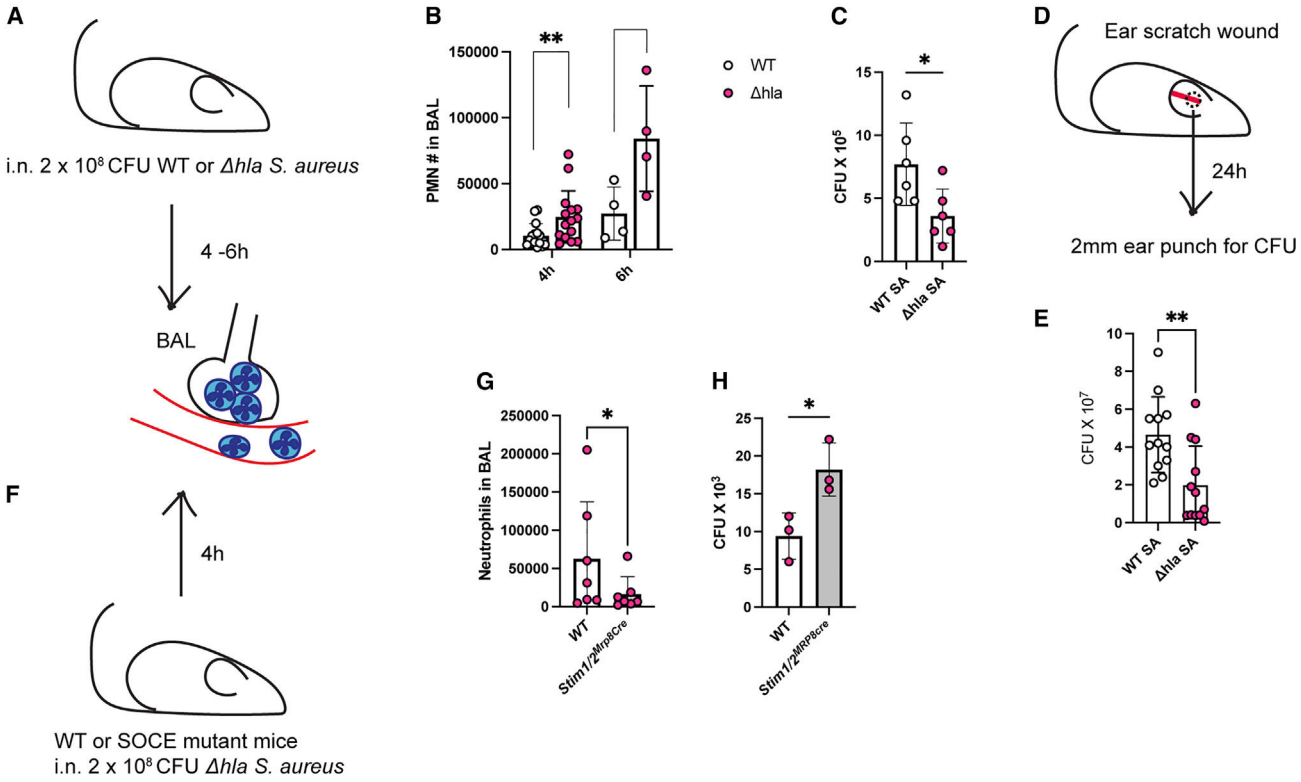

Figure 7. Hla impairs early neutrophil migration to the alveolus in lethal SA pneumonia

(A and B) WT or *Δhla* SA (2.4×10^8) was administered intranasally (A), and Ly6G+, CDllb+ neutrophil accumulation in the BAL was measured at 4–6 h using flow cytometry (B).

(C) Lungs from were digested at 4 hpi using collagenase, and SA CFUs were determined from the digestion using serial dilution. Data are representative of 4–15 mice compiled from 2–3 independent experiments.

(D and E) CFUs recovered from punch biopsies taken from WT or *Δhla* SA ear scratch wounds at 24 h after infection. Data for each SA genotype are representative of 12 scratch wounds in 6 mice, complied from 2 independent experiments.

(F–H) *Δhla* SA was administered intranasally to WT or *Stim1/2*^{MRP8Cre} mice, and BAL neutrophils and SA CFUs were quantified at 6 h. Data in (G) represent 7 mice compiled from 3 independent experiments. Data in (H) are a representative plot of 3 independent experiments. Data from experimental replicates were not combined here due to variability in the recovered bacteria between experiments.

(B) Two-way ANOVA. (C–H) Student's t test. *$p < 0.05$; **$p < 0.01$; ***$p < 0.001$; ****$p < 0.0001$. Error bars represent standard deviation.

Author Manuscript Author Manuscript Author Manuscript Author Manuscript

KEY RESOURCES TABLE

REAGENT or RESOURCE	SOURCE	IDENTIFIER
Antibodies		
Brilliant Violet 785™ anti-mouse Ly-6G (IA8) Antibody	BioLegend	BioLegend Cat# 127645, RRID:AB_2566317
Alexa Fluor® 647 Rat Anti-Mouse CD101 (Igsf2)	BD	BD Biosciences Cat# 564473, RRID:AB_2738821
Purified Rat Anti-Mouse CD16/CD32 (Mouse BD Fc Block™)	BD	BD Biosciences Cat# 553140, RRID:AB_394655
Bacterial and virus strains		
S. aureus USA300/LAC	Dr. Juliane Bubeck Wardenburg Washington University School of Medicine, St. Louis, MO. (Bubeck-Wardenburg et al.)	N/A
hla::erm S. aureus USA300/LAC	Dr. Juliane Bubeck Wardenburg Washington University School of Medicine, St. Louis, MO. (Bubeck-Wardenburg et al.)	N/A
S. aureus USA300/LAC YFP	Dr. Juliane Bubeck Wardenburg Washington University School of Medicine, St. Louis, MO. (Kwiecinski et al.)	N/A
Δhla S. aureus USA300/LAC YFP	Dr. Juliane Bubeck Wardenburg Washington University School of Medicine, St. Louis, MO. (Kwiecinski et al.)	N/A
Δhla S. aureus	This study	
Δhla/phla S. aureus	This study	
Δhla/pOS1 S. aureus	This study	
S. aureus USA300/LAC/pOS1 (WT/pOS1)	This study	
Chemicals, peptides, and recombinant proteins		
HBSS 1X	Corning	Cat# 21–022-CM
HBSS 10X	Gibco	Cat# 14185–052
PBS 1X	Corning	Cat# 21–040-CM
Cell Culture Grade Water	Corning	Cat# 25–055-CV
Percoll	Cytiva	Cat# 17089101
HEPES Buffer	Corning	Cat# 25–060-Cl
Ethanol	Decon Laboratories	Cat# 2701
NaCl	Sigma-Aldrich	Cat# S7653–250G
$MgCl_2$	Sigma-Aldrich	Cat# M2393–100G
$CaCl_2$	Millipore Sigma	Cat# 10035–04-8
ChCl	Sigma-Aldrich	Cat# C7527–100G
Sodium Bicarbonate	Sigma-Aldrich	Cat# S6297–250G
Trypan Blue Stain 0.4%	Invitrogen	Cat# T10282
Heat Inactivated Fetal Bovine Serum	Gibco	Cat# 16140–071
UltraPure Agarose	Invitrogen	Cat# 16500–100

Author Manuscript Author Manuscript Author Manuscript Author Manuscript

REAGENT or RESOURCE	SOURCE	IDENTIFIER
Tryptic Soy Agar	BD	Cat# 236950
Tryptic Soy Broth	Remel	Cat# R455052
EDTA, 0.5M	Corning	Cat# 46–034-Cl
Complement Component C5a	R&D	Cat# 2150-C5
LTB4	Cayman	Cat# 71160–24-2
Indo-1, AM	Invitrogen	Cat# 1223
Probenecid	Invitrogen	Cat# P36400
DAPI	Sigma-Aldrich	Cat# D9542
DiBAC4(3)	Invitrogen	Cat# B438
Zileuton	Sigma-Aldrich	Cat# Z4277–10MG
Collagenase D	Roche Diagnostics	Cat# 11088866001
DNase	Sigma-Aldrich	Cat# D5025
Hla - recombinant	Dr. Juliane Bubeck Wardenburg Washington University School of Medicine, St. Louis, MO	Ragle B. et al., Anti-alpha-hemolysin monoclonal antibodies mediate protection against *Staphylococcus aureus pneumonia. Infect Immun.* 2009; 77(7): 2712–2718.
Hla_{H35L} - recombinant	Dr. Juliane Bubeck Wardenburg Washington University School of Medicine, St. Louis, MO	Bubeck Wardenburg J. et al., Vaccine protection against *Staphylococcus aureus* pneumonia. *J Exp Med.* 2008; 205(2): 287–294.
Critical commercial assays		
μ-Slide Chemotaxis ibiTreat	Ibidi	Cat# 80326
LTB4 Parameter Assay Kit	R&D	Cat# KGE006B
EasySep Direct Human Neutrophil Isolation kit	Stem Cell	Cat# 19666
Experimental models: Organisms/strains		
Mouse: C57BL/6J	The Jackson Laboratory	Cat# 000664
Mouse: $Salsa6f^{flox/flox}$	The Jackson Laboratory	Cat# 031968
Mouse: Lyz2-Cre	The Jackson Laboratory	Cat# 004781
Mouse: MRP8-Cre	The Jackson Laboratory	Cat# 021614
Mouse: Vav-iCre	The Jackson Laboratory	Cat# 018968
Mouse: Lyz2-eGFP	Dr. Thomas Graf Albert Einstein College of Medicine, Bronx, NY	Faust N. et al., Insertion of enhanced green fluorescent protein into the lysozyme gene creates mice with green fluorescent granulocytes and macrophages. *Blood.* 2000; 96(2): 719–726[20]
Mouse: $Adam10^{flox/flox}$	Dr. Juliane Bubeck Wardenburg Washington University School of Medicine, St. Louis, MO	Inoshima N. et al., Genetic requirement for ADAM10 in severe Staphylococcus aureus skin infection. *J Invest Dermotol.* 2012; 132(5): 1513–1516[46]
Mouse: $Stim1^{flox/flox}$	Dr. Tomohiro Kurosaki RIKEN Research Center for Allergy and Immunology, Yokohama, Japan	Baba Y. et al., Essential function for the calcium sensor STIM1 in mast cell activation and anaphylactic responses. *Nat Immunol.* 2008; 9(1): 81–88[50]
Mouse: $Stim2^{flox/flox}$	Dr. Yoshihiro Baba Osaka University, Osaka, Japan	Matsumoto M. et al., The calcium sensors STIM1 and STIM2 control B cell regulatory function through

Author Manuscript Author Manuscript Author Manuscript Author Manuscript

REAGENT or RESOURCE	SOURCE	IDENTIFIER
		interleukin-10 production. *Immunity.* 2011; 34(5): 703–714[51]
Oligonucleotides - primers used for Hla allelic replacement		
GATTAAATTATTATAGCAATACTTTATTGTCC	Dr. Juliane Bubeck Wardenburg	Hla-X1
GTACATGAACAAATAATTTACATTAGTTTTA AAAAATAGAAG GATGATGAAAAT	Dr. Juliane Bubeck Wardenburg	Hla-X2
CATTTTCATCATCCTTCTATTTTTTAAAACTA ATGTAAATTATTTGTT CATGTAC	Dr. Juliane Bubeck Wardenburg	Hla-X3
GCTATCTTTAGTTTTAATATAAACTATTAGG	Dr. Juliane Bubeck Wardenburg	Hla-X4
TACATACGATACTTTTTCGTTATC	Dr. Juliane Bubeck Wardenburg	Hla-S1
GTTACAACCTCATGCTCTC	Dr. Juliane Bubeck Wardenburg	Hla-S2
Software and algorithms		
ImageJ	https://imagej.net/ij/index.html	RRID:SCR_003070
Chemotaxis and Migration Tool	https://ibidi.com/chemotaxis-analysis/171-chemotaxis-and-migration-tool.html	RRID:SCR_022708
Imaris	https://imaris.oxinst.com/	RRID:SCR_007370
GraphPad Prism 8	https://www.graphpad.com/scientific-software/prism/	RRID:SCR_002798
Motility Lab	http://2ptrack.net/	N/A
Other		
μ-Slide 8 well uncoated	Ibidi	Cat# 80821